Epitope-Driven Polyfunctional Divergence of SARS-CoV-2 RBD Antibodies

Pierre Rosenbaum[1], Cyril Planchais[1], Timothée Bruel[2], Maxime Beretta[1], Isabelle Staropoli[2], William-Henry Bolland[2], Florence Guivel-Benhassine[2], Delphine Planas[2], French COVID Cohort Study Group[#], CORSER Study Group[#], Olivier Schwartz[2], Hugo Mouquet[1,3*]

[1]Institut Pasteur, Université Paris Cité, Humoral Immunology Unit, Paris, France
[2]Institut Pasteur, Université Paris Cité, Virus & Immunity Unit, Paris, France
[3]Lead contact.

[#]The list of consortia members and affiliations appears at the end of the paper

*Correspondence: hugo.mouquet@pasteur.fr (H.M.).

SUMMARY

SARS-CoV-2 antibodies targeting the receptor binding domain (RBD) of the spike protein can potently neutralize infection and exert additional antiviral functions. Here, we characterize the functional profiles of human RBD-specific memory B-cell antibodies elicited by ancestral SARS-CoV-2 infection. While SARS-CoV2 neutralizing antibodies, mainly class 1 and 3 anti-RBD antibodies, often lose binding and neutralizing capacities against Omicron variants, most non-neutralizers remain broadly reactive. Despite their restricted cross-reactivity, neutralizing antibodies mediate Fc-effector functions including antibody-dependent cellular cytotoxicity, phagocytosis, and complement deposition. Most neutralizers also enhance binding of antibodies that target the SARS-CoV-2 spike fusion peptide *via* receptor-mimetic allostery. In contrast, broadly reactive non-neutralizers fail to trigger phagocytic or allosteric effects. Thus, viral escape compromises antibody neutralizing as well as other antiviral activities, leaving broadly reactive, non-polyfunctional antibodies that exert minimal immune pressure less effective at controlling infection.

15 **INTRODUCTION**

16 Humoral immune responses to SARS-CoV-2, most notably neutralizing antibodies, are
17 essential for protecting vaccinated and convalescent individuals from (re-)infection[1–3]. SARS-
18 CoV-2 neutralizing antibodies target multiple epitopes on three major regions of the viral spike
19 glycoprotein including the receptor-binding domain (RBD), N-terminal domain (NTD) and S2
20 stalk[4,5]. Anti-RBD neutralizers belong to six different classes, depending on their epitope
21 location - either within (class 1 and 2) or outside (class 3 to 6) the receptor-binding motif
22 (RBM)[6–8]. They are major contributors to seroneutralizing activity[9], and many have been
23 engineered as monoclonal antibodies for both prophylactic and therapeutic interventions
24 against COVID-19[10,11]. However, the antigenic drift resulting from the continuous evolution of
25 SARS-CoV-2 has severely compromised the effectiveness of both antibodies pre-existing in
26 immune donors and those used in clinics[12–17]. Novel anti-RBD neutralizing antibodies that were
27 more resilient to viral escape - such as SA55, VIR-7229 and VYD2311 - were advanced into
28 clinical development[18–20], but only SA55 remains potently active against the most recent post-
29 JN.1 variants[21]. Apart from neutralization, SARS-CoV-2 spike-specific antibodies can harbor
30 Fc-effector functions such as antibody-dependent cell cytotoxicity (ADCC), antibody-
31 dependent cell phagocytosis (ADCP) and complement dependent cytotoxicity (CDC), which
32 could contribute to SARS-CoV-2 infection control[22–31]. Infection and vaccination elicit SARS-
33 CoV-2 antibodies with Fc-dependent effector functions that persist over time[30–32]. Although
34 their exact roles remain to be fully elucidated, these functions may indeed be critical for viral
35 clearance, as exemplified by studies on class 3 antibody S309/Sotrovimab[33,34]. Certain anti-
36 RBD antibodies also exert allosteric effects by inducing conformational changes in the spike
37 protein that mimic the angiotensin converting enzyme 2 (ACE2) interaction, thereby enhancing
38 the potency of non-RBD neutralizing antibodies[35–37].

39 We previously uncovered a potential dichotomy in SARS-CoV-2 antibody-mediated
40 antiviral functions according to spike epitope specificity, with potent Fc-dependent effectors
41 mainly targeting the S2 subunit and NTD; however, only a small subset of anti-RBD
42 monoclonal antibodies were characterized in that study[38]. Here, to gain deeper insight into Fc-

43 effector antiviral mechanisms of anti-RBD antibodies, we generated a panel of human RBD-
44 specific monoclonal antibodies cloned from memory B cells of individuals who recovered from
45 ancestral SARS-CoV-2 infection. We characterized their reactivity and epitope profiles, as well
46 as their antiviral activities including neutralization, ACE2-mimetic effects, and Fc-dependent
47 effector functions. We showed that Omicron lineages preferentially evade polyfunctional class
48 1 anti-RBD neutralizers, reducing not only neutralization but also associated Fc-effector and
49 ACE2-mimetic allosteric activities, whereas the remaining broadly reactive non-neutralizing
50 anti-RBD antibodies have substantially diminished functional capacity.

51 **RESULTS**

52 **Human anti-RBD memory B-cell antibody profiles**

53 To select ancestral SARS-CoV-2-exposed convalescent donors (n=42 total) for single B-cell
54 antibody cloning, we first evaluated their IgG seroreactivity to recombinant Wuhan, Beta (β)
55 and Delta (δ) SARS-CoV-2 RBD proteins by ELISA (**Figs. 1A** and **S1A**). Peripheral blood IgG^+
56 and IgA^+ memory B cells from five donors with high serum anti-RBD antibody levels were
57 stained with fluorescently labeled β and δ RBD protein baits for flow cytometry phenotyping
58 and single-cell sorting (**Figs. 1B** and **S1B**). RBD-dual reactive class-switched memory B cells
59 ($RBD^{\beta\delta+}$) were detected at similar frequencies among donors (0.11±0.02%) and mainly
60 displayed a resting memory phenotype ($CD19^+CD27^+CD21^+$) (**Figs. 1B**, **1C**, **S1C** and **S1D**).
61 From single $RBD^{\beta\delta+}$-captured B cells, we produced 66 unique recombinant IgG1 monoclonal
62 antibodies by expression cloning[39] (originally, 49 IgG and 17 IgA as native isotype) (**Table S1**).
63 Among them, 84% (n=56) were specific based on high-affinity ELISA binding to Wuhan RBD,
64 and as expected, the vast majority also recognized both β and δ variant RBD proteins (84%,
65 n=47) (**Figs. 1D** and **1E**). Subsequent analyses were restricted to dual-reactive (β and δ) anti-
66 RBD antibodies and excluded Wuhan-monoreactive antibodies (n = 9). To assess their cross-
67 reactive potential against viral variants, we first performed ELISA and flow cytometry binding
68 analyses against 23 different SARS-CoV-2 RBD and/or S proteins (Alpha to Omicron BA.2.86).
69 About half of them (45%) showed pan-reactivity against pre- and post-omicron variants despite
70 being derived from memory B cells elicited by the ancestral strain (**Figs. 2A**, **S2A** and **Table**
71 **S2**). Some anti-$RBD^{\beta\delta}$ antibodies (17%, n=8) strongly cross-reacted with the SARS-CoV-1 tri-
72 S protein, but not with those of 229E, MERS-CoV, or HKU1 (**Fig. S2B**). Based on RBD-ELISA
73 competition assay using reference antibodies as potential competitors - REGN10987[40], CB6[41],
74 LY-CoV555[42], CT-P59[43], COV2-2130[44], ADG-2[45], Ly-CoV1404[13] and S309[46] - we categorized
75 the anti-RBD antibodies as class 1 (34%), class 2 (8.5%), class 3 (10.6%) or unclassified
76 (46.8%) (**Fig. 2B**). Antibodies with restricted binding profiles against RBD variants primarily
77 belonged to class 1 and 2 (81% and 75%, respectively), whereas those with broader reactivity

78 spectra were more frequently found in class 3 and unclassified groups (60% and 64%,
79 respectively) (**Figs. 2C, 2D** and **S2C**).
80
81 **Neutralizing and Fc-dependent effector activities of human anti-RBD antibodies**
82 We next evaluated the *in vitro* neutralizing capacity of anti-RBD antibodies against authentic
83 live viruses using the S-Fuse assay[47]. About half of them (n=20) showed significant neutralizing
84 activity against at least two variants in a pre-Omicron 5-viruses panel (D614G, α, β, γ, and δ),
85 with a quarter being active against all five viral strains (**Fig. 3A** and **Table S3**). Most cross-
86 neutralizers belonged to class 1 and 3 RBD antibodies (**Fig. S3A**). Comparable results were
87 observed using a virus like particles (VLP) reporter cell-based assay and an RBD-ACE-2
88 competitive ELISA[39], with blocking activity in the latter assay mainly restricted to class 1
89 antibodies, as anticipated (**Figs. 3A**, **S3A-C** and **Table S3**). We further examined the breadth
90 of the six most potent neutralizers (5 class 1 and a class 3) against 8 Omicron variants in the
91 S-Fuse assay (BA.1 to XBB.1.5). As previously observed for other class I such as Cv2.1169[48],
92 all lost their activity post-BA.2 excepted Cv2R.13162, which still neutralized SARS-CoV-2
93 variants up to XBB.1.5 (**Figs. S4A-D**). Noteworthy, antibodies with broad reactivity profiles on
94 pre- and Omicron RBD proteins were more frequently found among non-(cross)neutralizers as
95 compared to cross-neutralizing antibodies (70% *vs* 10%, p=0.0001) (**Figs. 3A** and **3B**). To
96 further investigate the antiviral properties of human SARS-CoV-2 RBD-specific antibodies, we
97 next assessed their *in vitro* capacity to mediate ADCC, ADCP and complement deposition
98 (CD) as a proxy for CDC. Most anti-RBD antibodies induced both ADCC and CD to varying
99 degrees, irrespective of whether their RBD reactivity spectra were narrowed or broad (**Figs.
100 3C**, **3D** and **Table S3**). In contrast, only few broadly RBD-reactive antibodies promoted ADCP,
101 compared with antibodies exhibiting limited cross-reactivity (9.5 % *vs* 54%, p=0.002) (**Figs.
102 3C**, **3D** and **Table S3**). Moreover, potent ADCP inducers were more frequently found among
103 class 1 RBD antibodies, the majority of which neutralized only pre-Omicron variants (**Fig. S3D
104** and **Table S3**). These data show that neutralizing anti-RBD antibodies can also serve as broad

105 Fc-dependent effectors, while broadly RBD-reactive antibodies are non-neutralizing, less
106 polyfunctional, but can still trigger ADCC and CD.
107
108 **ACE2-mimetic property of human anti-RBD antibodies**
109 Beyond direct antiviral effects, anti-RBD antibodies can allosterically or cooperatively enhance
110 the activity of other non-RBD antibodies[49–53]. Some of them increase S2 epitope accessibility,
111 thereby boosting the neutralizing capacity of anti-S2 antibodies, including those targeting the
112 FP[36,37]. Considering the potential *in vivo* relevance of cross-epitope antibody cooperativity and
113 synergy, we next examined whether anti-RBD antibodies could facilitate exposure of the FP
114 epitope. To this end, we produced four novel human anti-FP antibodies cloned from FP-
115 captured memory B cells of two selected convalescent donors with high serum anti-FP IgG
116 levels (**Figs. S5A-D**). Three of them (Cv2F.14107, Cv2F.14125, and Cv2F.14132) were clonal
117 variants from the same B-cell lineage, whereas the other (Cv2F.4147) was a unique clone
118 (**Table S1**). Despite their broad reactivity across coronaviruses, including SARS-CoV-2
119 variants, they showed little or no neutralizing activity against SARS-CoV-2, unlike previously
120 reported anti-FP antibodies 76E1, CoV4462 and C77G12[36,37,54] (**Figs. 4A** and **S5E-G**).
121 Following soluble ACE2 interaction, Cv2F.14107, but not Cv2F.4147, showed increased
122 reactivity to cell-expressed δ spike proteins (**Fig. 4B**), and was therefore used as a probe in
123 the flow cytometry binding assay to reveal allosteric effects of anti-RBD antibodies. Most
124 antibodies that enhanced Cv2F.14107 binding to the SARS-CoV-2 spike had narrow RBD
125 cross-reactivity (81% *vs* 14% for broad, $p<0.0001$) and, consequently, mainly belonged to
126 class 1 and neutralizer groups (**Figs. 4C**, **4D** and **S6A**). Nevertheless, some non-neutralizing
127 (Cv2R.13148, Cv2R.6151) and broadly reactive (Cv2R.12145, Cv2R.11176) antibodies also
128 triggered FP epitope exposure, indicating that this cooperative mechanism occasionally
129 extends beyond potent neutralizing, narrowly reactive, class 1 antibodies (**Figs. 4C**, **4D** and
130 **S6A**). We next examined the effects of anti-RBD antibodies at the polyclonal level using RBD-
131 enriched and -depleted IgG fractions from six convalescent donors. Although both fractions
132 bound to δ SARS-CoV-2 S proteins, only the RBD-enriched IgG antibodies enhanced

133 Cv2F.14107 recognition (in 4 out of 6 donors; **Fig. 4E**). As expected, enhanced Cv2F.14107
134 binding to the spike did not occur for BA.2.86 and EG.5.1, likely due to the poor reactivity of
135 anti-RBD antibodies against these variants (**Figs. S6B** and **S6C**). Principal component
136 analysis demonstrated clear segregation between anti-RBD with narrow and broad reactivity
137 based on antiviral functions (neutralizing, Fc-dependent effector and ACE2-mimetic activities)
138 (**Fig. 4G**), suggesting that anti-RBD antibodies are typically either broadly reactive or potent
139 polyfunctional immune effectors, but rarely both.
140

141 **Neutralizing activity of combined anti-RBD ACE2-mimetic and anti-FP antibodies**

142 Cv2R.12145 is a rare, pan-reactive class 1 antibody that modestly neutralized pre-BA.2 SARS-
143 2 variant (**Figs. 5A** and **5B**). Cv2R.12145 enhanced FP accessibility to Cv2F.14107 as
144 efficiently as soluble ACE2 and previously described ACE2-mimetic antibody CB6[36,55] (**Figs.**
145 **5C** and **S6D**). Unlike CB6, which lost its FP "unmasking" capacity against XBB.1.5, EG.5.1 and
146 BA.2.86 due to altered reactivity, Cv2R.12145 still bound these variants and facilitated their
147 recognition by Cv2F.14107 (**Figs. 5C** and **S7**). We next investigated whether combining
148 Cv2R.12145 with Cv2F.14107 would result in additive or synergistic effects in neutralizing
149 post-BA.1 variants. To this end, we conducted a synergy-scoring model analysis of *in vitro*
150 neutralization data obtained on BA.5 and EG.5.1, using VLP reporter cell-based and S-Fuse
151 assays, respectively. Antibodies in the cocktail showed no overall synergy, with total synergy
152 δ-scores of 4.2 and 2.2, respectively; global synergy is typically defined by a δ-score of >10
153 (**Figs. 6D** and **6E**). However, δ-scores nearly doubled withing specific high concentration
154 ranges for one or both antibodies (δ = 7.4 and δ = 4.25 for BA.5 and XBB.1.5, respectively)
155 (**Figs. 6D** and 6**E**). These results indicate that, while Cv2R.12145 enhances the binding of
156 Cv2F.14107 to SARS-CoV-2, their combined neutralization is primarily additive, with stronger
157 localized effects at high concentrations.

158 **DISCUSSION**

159 While neutralization by anti-spike antibodies is the primary protective mechanism against
160 COVID-19, their Fc-effector functions also contribute to immune protection, control, and
161 clearance of infection[32,56]. Fc-effector functions of antibodies are governed by the interplay
162 between paratope features (*i.e.*, epitope specificity and accessibility, binding affinity and
163 stoichiometry, and overall binding geometry and topology) and Fc region properties (*i.e.*,
164 isotype, subclass, glycosylation pattern)[57]. Fc-effector competent antibodies target multiple
165 regions of the viral spike, including the RBD[32,56]. Here, we functionally profiled a panel of RBD-
166 specific human monoclonal antibodies cloned from memory B cells of individuals infected with
167 ancestral SARS-CoV-2. RBD-captured memory B cells produced both neutralizing and non-
168 neutralizing antibodies. As expected from the escape and evolution[58,59], most neutralizing
169 antibodies lost their ability to bind and neutralize viruses in the Omicron lineage. Nonetheless,
170 we identified a resilient class 1 anti-RBD neutralizing antibody, Cv2R.13162 - reminiscent of
171 our previously reported broadly neutralizing antibody Cv2.3194[48,60] - that maintains activity
172 against Omicron variants up to XBB.1.5. Notably, class 1 neutralizing antibodies also mediated
173 ADCC, ADCP, and CD against ancestral SARS-CoV-2 *in vitro*. Among these, Cv2R.12145 and
174 Cv2.1176 stood out from the others by exhibiting broad reactivity against all RBD variants
175 tested. However, most class 1 neutralizers likely fail to elicit Fc-effector functions against
176 neutralization-resistant Omicron variants, as recently showed for infection- and vaccine-
177 induced class 1/2 anti-RBD antibodies[61]. On the other hand, the majority of antibodies binding
178 to non-neutralizing epitopes under lower selective pressure were cross-reactive against all
179 tested RBD variants. Despite absent or weak neutralization and ADCP, these cross-reactive
180 RBD-specific antibodies retained the capacity to induce CD and ADCC. Whether these anti-
181 RBD antibodies would contribute to *in vivo* protection and viral clearance following infection
182 with post-Omicron SARS-CoV-2 variants remains unclear. Notably, some vaccine-induced,
183 non-neutralizing anti-RBD antibodies that mediate ADCC but not ADCP or CD activity have
184 been shown to protect *in vivo* against lethal challenge with ancestral SARS-CoV-2[62]. More
185 generally, in animal models, optimal *in vivo* prophylactic and/or therapeutic efficacy of

186 neutralizing and non-neutralizing anti–SARS-CoV-2 antibodies, require intact Fc-mediated
187 effector functions[28,62–65]. ACE2-mimetic anti-RBD neutralizing antibodies have previously
188 shown to enhance anti-FP antibody reactivity and/or neutralization by inducing spike
189 conformational changes[49–51]. We further show that contrary to broadly reactive SARS-CoV-2
190 antibodies binding outside the RBM, most class 1 neutralizers enhance antibody recognition
191 of the FP on the spike protein. Combining the potent ACE2-mimetic Cv2R.12145 with the anti-
192 FP Cv2F.14107 markedly increased Cv2F.14107 binding to spike and produced additive
193 neutralization effects, but not the robust synergy previously reported for the anti-FP
194 C77G12/anti-RBD S2E12 and anti-FP 76E1/anti-RBD CB6 combinations[49,50]. This is likely due
195 to the low intrinsic potency of Cv2F.14107: despite targeting an epitope similar to 76E1, it
196 exhibits substantially reduced binding affinity and neutralizing activity against SARS-CoV-2.

197 Neutralizing antibodies impose strong selective pressure for viral escape, driving
198 SARS-CoV-2 evolution that culminated in the emergence of highly mutated Omicron
199 lineages[58]. As a result, potent anti-RBD neutralizers - particularly class 1 antibodies - have
200 largely lost their neutralization capacity against Omicron variants[66–69]. Our study suggests that
201 viral evolution did not only confer resistance to neutralization by class 1 antibodies, but also
202 more broadly compromised Fc effector and allosteric antiviral functions. Loss of these latter
203 activities may further reduce the protective efficacy of SARS-CoV-2 antibodies. Disruption of
204 Fc-mediated effector functions of anti-RBD neutralizing antibodies has been shown to
205 markedly impair their prophylactic and therapeutic efficacy in rodent models[56,63]. Thus, SARS-
206 CoV-2 can escape potent, polyfunctional neutralizers. In contrast, we show that anti-RBD
207 antibodies targeting epitopes outside the RBM, with broad recognition across Omicron
208 lineages, can still promote ADCC and complement deposition. This may explain why anti-RBD
209 antibody effector activities measured serologically in convalescents exposed to ancestral
210 SARS-CoV-2 are not completely abrogated against pre-Omicron variants[70]. Effector-
211 competent non-neutralizing antibodies, including those targeting the RBD, can efficiently
212 protect mice against SARS-CoV-2 infection[62,65]. It is generally accepted that Fc mediated
213 antibody effector functions play an important role once infection is established, but have a

214 more limited impact on sterilizing immunity than neutralization[31,32,56]. Whether cross-reactive,
215 non-neutralizing anti-RBD effector responses elicited by ancestral infection contribute
216 substantively to protection against Omicron-mediated COVID-19 remains unclear. Of note,
217 Wuhan-based vaccines that cross-protect against severe COVID-19 elicit anti-spike antibodies
218 with durable but variable Fc-effector activities[71], which appear to be largely preserved against
219 Omicron lineages, albeit to varying degrees depending on the specific variant[34,72,73].
220

221 **Limitations of the study**

222 We employed *in vitro* surrogate assays to evaluate the Fc-dependent effector functions of
223 human anti-RBD antibodies using ancestral SARS-CoV-2 proteins. Our data would benefit
224 from additional analyses using primary infected target and effector cells, inclusion of further
225 viral variants (*e.g.*, Omicron strains) and anti-RBD antibody classes, as well as *in vivo*
226 confirmation in relevant animal models. Assessing the *in vivo* Fc-mediated antiviral activities
227 of anti-RBD antibodies - including engineered variants with altered Fcγ receptor binding - may
228 provide valuable insights into the contribution of Fc-dependent effector functions to infection
229 protection and resolution. Although most anti-RBD monoclonals were produced as native
230 IgG1, we did not generate recombinant versions of non-IgG1 antibodies (*e.g.*, IgG3 and IgA1),
231 precluding assessment of Fc-dependent effector functions in their original subclass. In
232 addition, the glycosylation profiles of these recombinant antibodies may differ from those of
233 naturally produced IgGs, potentially modulating their Fc-effector activities.

RESOURCE AVAILABILITY

Lead Contact

Requests for resources and reagents should be directed to and will be fulfilled by the lead contact, Hugo Mouquet (hugo.mouquet@pasteur.fr).

Materials Availability

Request for reagents will be made available by the lead contact with a Material Transfer Agreement.

Data and code Availability

This paper does not report original code. Data used for the analysis is available in supplemental tables. Any additional information required to reanalyze the data reported in this paper is available from the lead contact upon reasonable request.

ACKNOWLEDGMENTS

We are grateful to all convalescent donors who consented to participate in this study, as well as to everyone who contributed to the CORSER and French COVID studies. We thank Sandrine Schmutz and Sophie Novault for their help with single-cell sorting (CB-UTechS, Institut Pasteur), and Dr Lubka Roumenina (Centre de Recherche des Cordeliers, France) for providing pre-pandemic sera for complement-related experiments. The French COVID Cohort, sponsored by the INSERM, was funded by the REACTing consortium, the Ministry of Health and Social Affairs, the Ministry of Higher Education and Research dedicated COVID-19 fund and Programme Hospitalier de Recherche Clinique (no. 20-0424). This work was supported by grants from the Agence Nationale de la Recherche REACTing COVID-19 (#20RR028-00), the European Commission Horizon 2020 program (RECoVER project, #101003589), the Institut Pasteur Task Force COVID-19 (2019-NCOV THERAMAB project), and the Fondation de France (#00106077). P.R was supported by a two-years Pasteur-Roux-Cantarini fellowship (Institut Pasteur).

AUTHOR CONTRIBUTIONS

262 H. M. conceived and supervised the study. P. R., C. P., T. B., M. B., W.H. B., I. S., F. G., and
263 O. S., H. M. performed and/or analyzed the experiments. French COVID and CORSER Cohort
264 Study Groups provided human samples. P. R. and H.M wrote the manuscript with contributions
265 from all the authors.
266

267 **DECLARATION OF INTERESTS**

268 H.M. is the acting CSO of SpikImm biotech, for which he received consulting fees not related
269 to the present work.
270

271 **SUPPLEMENTAL INFORMATION**

272 Figures S1-S7 and Table S1-S3.

FIGURE LEGENDS

Figure 1. Human SARS-CoV-2 RBD-specific memory B-cell antibodies.
(**A**) 3D plot comparing the IgG seroreactivity of COVID-19 convalescent individuals (n=42) against purified Wuhan (Wu.), Beta (β), and Delta (δ) RBD proteins. Labeled, circled dots indicate donors selected for single memory B-cell flow cytometry sorting. Dots are color-coded according to their ELISA reactivity measured as areas under curve (AUC).
(**B**) Flow-cytometric plots showing circulating blood RBD-dual reactive ($RBD^{\beta\delta+}$) IgG^+ and IgA^+ memory B cells (gated as indicated in Fig. S1B) from the 5 selected convalescent donors.
(**C**) Donut charts comparing the phenotypic distribution of IgG^+ and IgA^+ memory B cells from which anti-RBD antibodies have been cloned (total cloned antibodies *per* donor are indicated in the center of the charts: B_{RM} (resting memory, $CD27^+CD21^+$), B_{AM} (activated memory, $CD27^+CD21^-$), and B_{TLM} (tissue-like memory, $CD27^-CD21^-$). Value at the center of each chart represents the total amount of antibodies *per* donor.
(**D**) Bubble plot comparing the ELISA reactivity of human $RBD^{\beta\delta+}$-captured memory B-cell antibodies against RBD Delta (δ, x axis), RBD Beta (β, y axis) and tri-S Wuhan (bubble size). OD, optical dentities. Antibodies were categorized as dual (yellow; OD > 1 for both RBD β and RBD δ), variant-specific (black; OD > 1 for RBD β or RBD δ), and not reactive (gray; OD < 1 for all RBDs).
(**E**) Donut charts comparing the distribution of anti-RBD antibody profiles based on the ELISA reactivities measured in Fig.1D. Total cloned antibodies *per* donor are indicated in the center of the charts.

Figure 2. Reactivity profiles of human anti-RBD antibodies.
(**A**) Heatmap (left) comparing the ELISA binding profiles of human anti-RBD antibodies (n = 47) against purified recombinant SARS-CoV-2 Wuhan (Wu.) tri-S, S1 and RBD proteins from various viral variants. Cells are color-coded according to mean OD values obtained with antibodies at 1 µg/ml. Antibodies were categorized as either broadly reactive (red) or with a more restricted cross-reactivity (grey). Graph (right) showing the proportion of antibodies in each category).
(**B**) Heatmap showing competition for Wuhan RBD binding of anti-RBD antibodies in the presence of reference antibodies as potential competitors: CT-P59, Cv2.1169, and CB6 (class 1); LyCoV555 (class 2); REGN10987, LyCoV1404, CoV2-2130 and S309 (class 3); ADG-2 (class 4). Cells are color-coded based on the binding inhibition relative to reactivity in absence of potential competitor (% bind.); dark blue corresponds to high binding inhibition, while white indicates no competition. Mean of duplicates values are shown.
(**C**) Donut charts comparing the frequency of broadly reactive (red) and restricted cross-reactive (gray) antibodies for each RBD class identified in (B) (1, 2, 3 and undefined). Total number of antibodies in each group is indicated in the center of the charts.
(**D**) Graph comparing the reactivity profiles of anti-RBD antibodies against SARS-CoV-2 RBD proteins from Wuhan and Omicron variants according to their class as defined in (B). Antibodies were considered reactive when OD > 2, and their proportion (%) is depicted (y axis).

Figure 3. Neutralizing and Fc-dependent effector activities of human anti-RBD antibodies
(**A**) Heatmap comparing the *in vitro* neutralization activity of human anti-RBD antibodies against SARS-CoV-2 D614G, Alpha (α), Beta (β), Gamma (γ) and Delta (δ) viruses using the S-fuse, virus-like particles (VLP) neutralization assays, and ACE2-tri-S or -RBD blocking ELISA assay. Dark blue colors indicate strongest inhibition percentages, while white corresponds to no inhibition. Mean of duplicate values are shown. Antibodies were categorized as either cross-neutralizing (dark pink), neutralizing (pink) or weak or non-neutralizing (white).
(**B**) Graph comparing the proportion of anti-RBD antibodies active in the S-Fuse, VLP, and ACE2/tri-S|RBD assays according to their reactivity profiles as defined in Fig. 2A. Antibodies were considered active when inhibition/neutralization % > 50%.

(**C**) Bar graphs comparing the ADCC, CD, and ADCP activities of anti-RBD antibodies (n=47). Bars are colored-coded based on antibody reactivity profiles. Data represents the mean± SD of duplicates from two independent experiments. Dotted lines represent positivity threshold based on the negative control.
(**D**) Scatter plots comparing the ADCC, CD and ADCP scores of anti-RBD antibodies according to their reactivity profiles (broad, n=21 and restricted, n=26). Groups were compared using Mann-Whitney's test.

Figure 4. ACE2-mimetic activity of anti-RBD antibodies
(**A**) Graph comparing the reactivity of human anti-FP antibodies Cv2F.4147 and Cv2F.14107 against 293F-cell transfectants expressing the spike proteins from various SARS-CoV-2 variants. Ctr corresponds to the non-transfected cell control. Data represent means ± SD of duplicate values of the geometric mean fluorescence intensities (gMFI) fold increase compared to no antibodies.
(**B**) Representative flow cytometry histograms (top) and bar graph (bottom) showing the flow cytometry binding of anti-FP antibodies to Delta spike-expressing 293F cells in the presence or absence of soluble recombinant ACE2 protein. Error bars in the graph represent the SD duplicate values for the fold increase (FI) of gMFI AUC compared to the no antibody condition.
(**C**) Bar graph comparing the binding enhancement of anti-FP antibody Cv2F.14107 to Delta spike-expressing 293F cells in the presence of human anti-RBD antibodies. Data represent the mean ± SD of duplicate values. Dotted lines indicate the basal gMFI (black) and a two-fold increase (blue). Antibodies are ordered according to their ability to potentiate the binding of anti-FP antibody and are color-coded by group: broad- (red) or restricted- (gray) reactivity (defined in Fig. 2A), references (pink), non-RBD reactive (green), and controls (black).
(**D**) Scatter plot (left) comparing the enhanced binding of Cv2F.14107 to spike measured in (C) according to the reactivity profiles of anti-RBD antibodies (broad, n=21 or restricted, n=26). Groups were compared using Mann-Whitney's test. Donut charts (right) comparing the potency of anti-RBD antibodies to increase Cv2F.14107 binding (high >2; none or low ≤ 2 FI gMFI) according to their reactivity profiles.
(**E**) Bar graphs comparing the Spike reactivity (left) and ACE2-mimetic capacity (right; enhanced Cv2F.14107 binding) measured by flow cytometry of total anti-RBD (blue) and non-RBD (grey) IgG antibodies purified from convalescent sera. Error bars represent the SD of duplicate values.
(**F**) PCA 2D-plot showing the antiviral-related variables (arrows) discriminating human anti-RBD antibodies (n = 47). Dots represent single antibodies, color-coded based their reactivity profiles.

Figure 5. SARS-CoV-2 binding and neutralization by combined Cv2R.12145 and Cv2F.14107 antibodies
(**A**) Representative ELISA graph showing the binding curves of anti-RBD antibody Cv2R.12145 to purified RBD proteins from Delta and Omicron variants. Error bars represent the SD of duplicate values.
(**B**) Graph showing the S-Fuse neutralization curves of Cv2R.12145 against SARS-CoV-2 D614G, Delta and Omicron variants. Error bars represent the SD of duplicate values from two intendent experiments.
(**C**) Representative flow cytometry histograms (left) and bar graph (right) comparing the Delta spike binding and ACE2-mimetic capacity (right; enhanced Cv2F.14107 binding) of soluble recombinant ACE2 ectodomain, and anti-RBD antibodies Cv2R.12145 and CB6. Error bars in the graph represent the SD duplicate values.
(D) Synergy maps (left) calculated on the dose-response neutralization matrices (heatmaps, right) of combined Cv2F.14107 and Cv2R.12145 against BA.5 using the VLP neutralization assay. Synergistic area are shown in red. Blue dotted square represent the highest synergy score (δ score). Global and highest local area synergy scores are indicated on each map.
(E) Same as in (D) but for EG.5.1 viruses in the S-Fuse assay.

STAR★METHODS

EXPERIMENTAL MODEL AND SUBJECT DETAILS

Human samples

Biobanked blood-derived samples from Wuhan COVID-19 convalescent donors (n=42) were previously obtained from the CORSER and French COVID cohorts[38]. These samples were collected from participants infected during the first the first epidemic wave in France, with blood sampling conducted in April 2020. Both cohorts were established in accordance with French legislation and regulations and following ethical approval from the relevant authorities. The CORSER study (NCT04325646) received ethical approval from the Comité de Protection des Personnes Ile-de-France III. The French COVID study was approved by the regional institutional review board (Comité de Protection des Personnes Ile-de-France VII, Paris, France) and conducted in accordance with European guidelines and the Declaration of Helsinki. All participants provided written informed consent to participate in this study, and data were collected in a pseudo-anonymized form using subject codes.

METHOD DETAILS

Viruses

Titrated SARS-CoV-2 viral stocks for the following strains used in the *in vitro* S-Fuse neutralization assay were prepared in the Viral and Immunity Unit (Institut Pasteur) as previously described[69,74–78]: D614G (hCoV-19/France/GE1973/2020; GISAID ID: EPI_ISL_414631) BetaCoV/France/IDF0372/2020 (GISAID ID: EPI_ISL_406596) (National Reference Centre for Respiratory Viruses, Institut Pasteur), α (GISAID ID: EPI_ ISL_735391), β (B.1.351; GISAID ID: EPI_ISL_964916), γ variant (P.1.; hCoV-19/Japan/TY7-501/2021; GISAID ID: EPI_ISL_833366)[79] δ (B.1.617.2; GISAID ID: EPI_ISL_2029113), BA.1 (GISAID ID: EPI_ISL_6794907), BA.2 (GISAID ID: EPI_ISL_10654979), BA.5 (GISAID ID: EPI_ISL_13660702), BA.2.75.2 (GISAID ID: EPI_ISL_15731524), BA.4.6 (GISAID ID: EPI_ISL_15729633, BQ.1.1 (GISAID ID: EPI_ISL_15731523, XBB.1 (GISAID ID: EPI_ISL_15619797), XBB.1.5 (GISAID ID: EPI_ISL_1635849) and EG.5.1 (GISAID ID: EPI_ISL_17949406).

Viral proteins and peptides

Codon-optimized nucleotide fragments encoding SARS-CoV-2 S2 subunit deleted from the FP, HR2, or SH domain, followed by a Foldon trimerization motif and C-terminal tags (8xHis-tag, Strep-tag, and AviTag) were synthesized and cloned into pcDNA3.1/Zeo(+) expression vector (Thermo Fisher Scientific). Already cloned pcDNA3.1/Zeo(+) vectors coding for the following tagged proteins were used to produce recombinant proteins by transient transfection of exponentially growing Freestyle 293-F suspension cells (Thermo Fisher Scientific) as previously described[80]: SARS-CoV-2, SARS-CoV-1, MERS-CoV, HKU1-CoV, 229E-CoV, SARS-CoV-2 BA.1 spike (HexaPro; S_6P; S) ectodomains; SARS-CoV-2 S2 subunit; tagged Wuhan, BA.1, BA.2, BA.2.12.1, BA2.75, BA2.75.2, BA.3, BA4/5, BA4.6, BF.7, BQ.1, BQ.1.1, XBB.1, XBB.1.16, XBB.1.5, and BA.2.86 RBD proteins. Proteins were purified from culture supernatants by high performance chromatography using the Ni Sepharose Excel Resin according to the manufacturer's instructions (GE Healthcare), dialyzed against PBS using Slide-A-Lyzer dialysis cassettes (Thermo Fisher Scientific), quantified using NanoDrop 2000 instrument (Thermo Fisher Scientific). AviTagged tri-S and RBD proteins were biotinylated using the Enzymatic Protein Biotinylation Kit (Sigma-Aldrich) following the manufacturer's instructions. For single B-cell FACS sorting, biotinylated RBD-β and RBD-δ proteins were coupled with respectively PE- and APC-conjugated streptavidin (Thermo Fisher Scientific), respectively; biotinylated fusion peptide (FP-biot; KRSFIEDLLFNKVTLADAGFIK, GenScript Biotech) was coupled to both. The library of 15-mer alanine-mutated SARS-CoV-2 FP (original

reference: KRSFIEDLLFNKVTL, n=15), and FP from SARS-CoV-2 (PSKRSFIEDLLFNKVTLADA), SARS-CoV-1 (PTKRSFIEDLLFNKVTLADA), HCoV-229E (VAGRSAIEDILFSKIVTSGL), MERS-CoV (RSARSAIEDLLFDKVTIADP), HCoV-HKU1 (SSRSLLEDLLFNKVKLSDV), SADS-CoV (FESRSVIEDLLFSKIETTGP), HCoV-NL63 (IAGRSALEDLLFSKVVTSGL), HCoV-OC43 (ASSRSAIEDLLFDKVKLSDV), CCov-HuPn-2018 (RKYRSAIEDLLFDKVVTSGL), IBV-9203 (PRRRSFIEDLLFTSVESVGL) and Hu-PDCoV (LGGRSAIEDLLFNKVVTSGL) were synthetized and desalted (GenScript Biotech).

Reference and control antibodies

Purified parental research IgG1 versions of benchmarked anti-RBD antibodies (REGN10987[40], CB6[41], LY-CoV555[42], CT-P59[43], COV2-2130[44], ADG-2[45], Ly-CoV1404[13] and S309[46]), anti-FP antibodies (C77G12[37], 76E1[36], CoV44-62[54]) were produced as described below following cloning of synthetic DNA fragments encoding immunoglobulin variable domains (Thermo Fisher Scientific). Non-SARS-CoV-2 antibody mGO53[81] (non-polyreactive) was used as a negative control.

Single B-cell FACS sorting and expression-cloning of antibodies

Human B cells were isolated from biobanked PBMCs using human CD19 MACS following manufacturer's procedures (Miltenyi Biotec). B cells were simultaneously incubated for 30 min at 4°C with an extemporaneously prepared mix of PE-coupled RBD-β and APC-coupled RBD-δ proteins (2 µg each) or with PE- and APC-coupled FP (2 µg each). Cells were washed once with 1% FBS-PBS (FACS buffer), stained using LIVE/DEAD aqua fixable dead cell stain kit (Molecular Probes; Thermo Fisher Scientific) and incubated 30 min with a cocktail of mouse anti-human antibodies: CD19 Alexa 700 (HIB19; BD Biosciences), CD21 BV711 (or BV421; B-ly4; BD Biosciences), CD27 PE-CF594 (M-T271; BD Biosciences), IgG BV786 (G18-145; BD Biosciences), IgA FITC (IS11-8E10; Miltenyi Biotec), and β7 integrin BV421 (or BUV395; FIB504, BD Biosciences). Cells were then washed and resuspended in 1 mM EDTA FACS buffer. Single alive RBDβ/δ$^+$CD19$^+$IgA$^+$ or IgG$^+$ and PE/APC-FP$^+$CD19$^+$IgG$^+$ cells were sorted into 96-well PCR plates using either a FACSAria Fusion or a FACSymphony™ S6 cell sorter (Beckton Dickenson). Single-cell cDNA synthesis using SuperScript IV reverse transcriptase (Thermo Fisher Scientific) followed by nested-PCR amplifications of IgH, Igκ, and Igλ genes were performed as previously described[82,83]. Purified digested PCR products were cloned into human Igγ1-, Igκ-, or Igλ-expressing vectors (GenBank# LT615368.1, LT615369.1, and LT615370.1, respectively), as previously described[83]. Recombinant antibodies were produced by transient co-transfection of Freestyle 293-F suspension cells (Thermo Fisher Scientific) using the PEI precipitation method[80]. Recombinant human IgG1 antibodies were purified by affinity chromatography using Protein G Sepharose 4 Fast Flow (GE Healthcare), and dialyzed against PBS. Cv2F.4147, Cv2F.14107 and 76E1 variable domain genes were also cloned into human Igα1- and Fab-Igγ1-expressing vector[80].Recombinant human IgA antibodies and Fab were purified by affinity peptide M-coupled agarose beads (Invivogen) and Ni Sepharose® Excel Resin (GE Healthcare), respectively.

ELISAs

ELISAs were performed as previously described[38,60]. Briefly, high-binding 96-well ELISA plates (Costar; Corning) were coated overnight with purified recombinant viral proteins (125 ng/well in PBS). After washings with 0.05% Tween 20-PBS (washing buffer), plates were blocked for 2 h with 2% BSA, 1 mM EDTA, 0.05% Tween 20-PBS (Blocking buffer), washed, and incubated with serially diluted human sera (1:100 and 3 consecutives 1:10 dilutions) or recombinant antibodies in PBS. For binding screening, anti-RBD antibodies were tested in triplicate at 1 µg/ml. Selected anti-RBD and anti-FP IgG antibodies were evaluated at 10 µg/ml followed by seven consecutives 1:4 and 1:10 dilutions in PBS, respectively. After washings, plates were revealed by incubation for 1 h with goat HRP-conjugated anti-human IgG (Jackson ImmunoReseach, 0.8 µg/ml final) and by adding 100 µl of HRP chromogenic substrate (ABTS

solution, Euromedex) after washing steps. Optical densities were measured at 405nm (OD405nm), and background values given by incubation of PBS alone in coated wells were subtracted. Experiments were performed using HydroSpeed™ microplate washer and Sunrise™ microplate absorbance reader (Tecan Männedorf, Switzerland). For peptide-ELISA, anti-FP and control IgG antibodies were tested at 10 µg/ml and three consecutive 1:10 dilutions in 1% BSA, 0.1% Tween 20-PBS using the same procedure as previously described[38,60]. For the competition experiments, Wuhan RBD-coated plates were blocked, washed and then incubated for 2 h with biotinylated antibodies at a concentration of 25 ng/ml in the presence of IgG1 antibodies as potential competitors at 50 µg/ml, all performed in duplicate. After washings, plates were developed by adding HRP-conjugated streptavidin (1:2000 dilution, BD Biosciences) for 30 min and ABTS solution as described above. The percentage of competition was calculated as follows: $100 \times [1- (OD^{bio\text{-}IgG+comp} / OD^{bio\text{-}IgG})]$.

Flow cytometry binding assay

Freestyle 293-F were transfected with pUNO1-Spike-dfur (Spike, SpikeV1 to V13 plasmids; Invivogen) and XBB.1.5, BA.2.86, EG.5.1 pHCMV expression vectors[78] (1.2 µg plasmid DNA *per* 10^6 cells) using the PEI-precipitation method. Forty-eight hours post-transfection, 0.3×10^6 transfected and non-transfected control cells were incubated with IgG antibodies for 30 min at 4°C (1 µg/ml). For the assessment of anti-FP binding, transfected and non-transfected cells were incubated with anti-RBD and control antibodies (at 10 µg/ml) in presence the presence of Dy650 labeled-ACE2 or -FP antibodies - labeled using the Dylight 650 NHS ester kit (Thermo Scientific) - in 2 mM EDTA, 5% FBS-PBS for 2 h at room temperature. After washings, cells were incubated for 20 min at 4°C with AF647-conjugated goat anti-human IgG antibodies (1:1,000 dilution; Thermo Fisher Scientific) and LIVE/DEAD Fixable Viability dye Aqua (1:1,000 dilution; Thermo Fisher Scientific), washed and resuspended in PBS–paraformaldehyde 1% (Electron Microscopy Sciences). Data were acquired using a CytoFLEX flow cytometer (Beckman Coulter) and analyzed by FlowJo software (v10.8; FlowJo LLC). Fold increase in binding for anti-FP IgG antibodies was determined as follow: $gMFI\text{-}APC^{IgG + anti\text{-}RBD \text{ or } ACE2} / gMFI\text{-}APC^{IgG \text{ alone}}$.

ACE2 binding inhibition assay

ELISA plates (Costar, Corning) were coated overnight with 250 ng/well of purified ACE2 ectodomain[38], washed and blocked with ELISA blocking solution. For pre-Omicron variants, biotinylated tri-S (1 µg/ml in PBS) and RBD (2 µg/ml in PBS) proteins were incubated in the presence of antibodies at 2 µg/ml and 20 µg/ml, respectively. For Omicron variants, biotinylated RBD proteins (2 µg/ml in PBS) were incubated in the presence of antibodies at 200 µg/ml. After washing, plates were revealed by a 30 min-incubation with HRP-conjugated streptavidin (1:1000 dilution; BD Biosciences), followed by PBST washes and addition of ABTS solution. Percentage of inhibition (%) was calculated using the following formula: $[1 - (OD^{RBD+mAb} / OD^{RBD})] \times 100$.

Viral-like particle neutralization assay

SARS-CoV-2 HiBiT-PsVLP Assay (Promega) was performed according to the manufacturer's instructions. Briefly, SARS-CoV-2 HiBiT-PsVLPs mixed with antibodies (1 µg/ml for D614G and 10 µg/ml for BA.1 and BA.5) were incubated for 30 min at 37°C. Antibody-VLP complexes were then added to HEK293T LgBit cells in the presence of DrkBit Peptide followed by a 3 h incubation. Nano-Glo® Live Cell Reagent was added to the cells and after 15 min incubation, bioluminescence signals (RLU) were measured using a SAFAS Xenius plate reader (SAFAS Monaco). Percentage inhibition (%) was calculated as follows : $100 \times [1 - (RLU^{mAb}/ RLU^{no\ mAb}]$.

SARS-CoV-2 S-Fuse neutralization assay

S-Fuse cells (1:1 mix of U2OS-ACE2-GFP1-10 and U2OS-ACE2-GFP11) were prepared and plated at a density of 2 x 104 per well in a µClear 96-well plate (Greiner Bio-One) as previously described[77]. SARS-CoV-2 virions (MOI 0.1) were incubated with antibodies at concentrations of 1 µg/ml for pre-Omicron variants and 10 µg/ml for Omicron variants in culture medium for

30 min at room temperature and then added to S-Fuse cells. For the most potent neutralizing antibodies, testing was performed at a starting concentration of 9 µg/ml, followed by 11 consecutive 1:4 serial dilutions. Cells were fixed 18 h later with 4% paraformaldehyde, washed, and stained with Hoechst dye (dilution 1:10,000; Invitrogen). Images were acquired with an Opera Phenix high-content confocal microscope (Perkin Elmer). The area of GFP-positive cells and the number of nuclei were quantified using with Harmony software 4.8 (Perkin Elmer). The neutralization % was calculated from the number of syncytia as follows: 100 × (1 - (value with IgG - value in "non-infected") / (value in "no IgG" - value in "non-infected")). IC_{50} values were calculated using Prism software (v.9.3.1, GraphPad Prism Inc.) by fitting replicate values using the four-parameters dose–response model (variable slope).

ADCP assay

PBMCs were isolated from healthy donors' blood (Etablissement Français du Sang) using Ficoll Plaque Plus (GE Healthcare). Primary human monocytes were purified from PBMCs by MACS using Whole Blood CD14 MicroBeads (Miltenyi Biotech). Biotinylated Wuhan SARS-CoV-2 tri-S proteins were incubated with FluoSpheres™ NeutrAvidin™ beads (1 µm, yellow-green (505/515); Thermo Fisher Scientific; 20 µg of tri-S for 2 µl of beads), washed, and incubated for 30 min at room temperature. After PBS washes, tri-S-coupled beads 1:10000-diluted in DMEM were incubated for 1 h at 37°C with human IgG1 antibodies (at 5 µg/ml). The tri-S-bead-antibody mixtures were then incubated with $1x10^5$ human monocytes for 2 h at 37°C. 0.5% BSA, 2 mM EDTA, PBS solution, cells were fixed with 4% PFA–PBS and analyzed using a CytoFLEX flow cytometer (Beckman Coulter). ADCP experiments were analyzed using the FlowJo software (v10.8; FlowJo LLC). ADCP score corresponds to the percentage of FITC-positive cells.

ADCC assay

The ADCC activity of anti-RBD antibodies IgG antibodies was determined using the ADCC Reporter Bioassay (Promega) according to the manufacturer's instructions. Briefly, $1x10^5$ Wuhan tri-S-transfected HEK293F cells were co-cultured with $6x10^4$ Jurkat-CD16-NFATrLuc cells in the presence or absence of anti-RBD or control mGO53 IgG antibody at 10 µg/ml. Luciferase was measured after 16 h of incubation using an GloMax Discoverer® plate reader (Promega). ADCC was measured as the fold induction of luciferase activity compared with the control antibody mGO53.

CD assay

The complement deposition (CD) of anti-RBD antibodies on Wuhan SARS-CoV-2 triS-expressing 293F cells was measured as previously described[84]. Briefly, $2x10^5$ triS-expressing 293F cells were cultivated in the presence of 50% normal or heat-inactivated human serum, and with or without IgG antibodies at 10 µg/ml. After 24 h, cells were washed with PBS and incubated for 30 min at 4°C with the live/dead fixable aqua dead cell marker (1:1,000 in PBS; Life Technologies) and PE-conjugated mouse anti-C3/C3b/iC3b IgG (2 µg/ml, 6C9; BD Biosciences) before fixation. Data were acquired using a CytoFLEX flow cytometer (Beckman Coulter) and analyzed using FlowJo software (v10.3; FlowJo LLC). CD scores were calculated by dividing the gMFI of live cells with mAb and normal serum by the gMFI of live cells without mAb.

QUANTIFICATION AND STATISTICAL ANALYSIS

B-cell immunophenotyping and quantification of B-cell subset frequencies were performed using FlowJo software (v10.8; FlowJo LLC). Antibody classes were compared for functional data (neutralization, Fc-effector functions) using two-tailed Mann-Whitney test for total individual values and with Chi-square test with Yates' correction for group frequencies. Statistical analyses were performed using GraphPad Prism software (v.8.2; GraphPad Prism Inc.). Heatmap representations were generated using GraphPad Prism or complex heatmap R package (v2.10.0; https://www.bioconductor.org/packages/release/bioc/html/ComplexHeat

map.html). PCA plots were generated using the factoextra package (v1.0.7; https://CRAN.Rproject.org/package=factoextra). The quantification of the synergistic effect and corresponding synergy map representations for antibody combinations was calculated using the SynergyFinder web application (v3.0) with the corrected Zero interaction potency (ZIP) model (https://synergyfinder.fimm.fi).

600 **REFERENCES**

601 1. Barouch, D.H. (2022). Covid-19 Vaccines — Immunity, Variants, Boosters. New England Journal of
602 Medicine *387*, 1011–1020. https://doi.org/10.1056/nejmra2206573.

603 2. Qi, H., Liu, B., Wang, X., and Zhang, L. (2022). The humoral response and antibodies against SARS-CoV-
604 2 infection. Nat. Immunol. *23*, 1008–1020. https://doi.org/10.1038/s41590-022-01248-5.

605 3. Röltgen, K., and Boyd, S.D. (2024). Antibody and B Cell Responses to SARS-CoV-2 Infection and
606 Vaccination: The End of the Beginning. Annual Review of Pathology: Mechanisms of Disease *19*, 69–97.
607 https://doi.org/10.1146/annurev-pathmechdis-031521-042754.

608 4. Errico, J.M., Adams, L.J., and Fremont, D.H. (2022). Antibody-mediated immunity to SARS-CoV-2 spike.
609 In Advances in Immunology https://doi.org/10.1016/bs.ai.2022.07.001.

610 5. Chen, Y., Zhao, X., Zhou, H., Zhu, H., Jiang, S., and Wang, P. (2023). Broadly neutralizing antibodies to
611 SARS-CoV-2 and other human coronaviruses. Nat. Rev. Immunol. *23*, 189–199.
612 https://doi.org/10.1038/s41577-022-00784-3.

613 6. Barnes, C.O., Jette, C.A., Abernathy, M.E., Dam, K.-M.A., Esswein, S.R., Gristick, H.B., Malyutin, A.G.,
614 Sharaf, N.G., Huey-Tubman, K.E., Lee, Y.E., et al. (2020). SARS-CoV-2 neutralizing antibody structures
615 inform therapeutic strategies. Nature *588*, 682–687. https://doi.org/10.1038/s41586-020-2852-1.

616 7. Rouet, R., Henry, J.Y., Johansen, M.D., Sobti, M., Balachandran, H., Langley, D.B., Walker, G.J., Lenthall,
617 H., Jackson, J., Ubiparipovic, S., et al. (2023). Broadly neutralizing SARS-CoV-2 antibodies through
618 epitope-based selection from convalescent patients. Nat. Commun. *14*, 687.
619 https://doi.org/10.1038/s41467-023-36295-5.

620 8. Chen, Y., Zhao, X., Zhou, H., Zhu, H., Jiang, S., and Wang, P. (2022). Broadly neutralizing antibodies to
621 SARS-CoV-2 and other human coronaviruses. Nat. Rev. Immunol. *4*. https://doi.org/10.1038/s41577-022-
622 00784-3.

623 9. Piccoli, L., Park, Y.J., Tortorici, M.A., Czudnochowski, N., Walls, A.C., Beltramello, M., Silacci-Fregni, C.,
624 Pinto, D., Rosen, L.E., Bowen, J.E., et al. (2020). Mapping Neutralizing and Immunodominant Sites on the
625 SARS-CoV-2 Spike Receptor-Binding Domain by Structure-Guided High-Resolution Serology. Cell *183*,
626 1024-1042.e21. https://doi.org/10.1016/j.cell.2020.09.037.

627 10. Corti, D., Purcell, L.A., Snell, G., and Veesler, D. (2021). Tackling COVID-19 with neutralizing monoclonal
628 antibodies. Cell *184*, 3086–3108. https://doi.org/10.1016/j.cell.2021.05.005.

629 11. Gruell, H., Vanshylla, K., Weber, T., Barnes, C.O., Kreer, C., and Klein, F. (2022). Antibody-mediated
630 neutralization of SARS-CoV-2. Immunity *55*, 925–944. https://doi.org/10.1016/j.immuni.2022.05.005.

631 12. Wang, Q., Iketani, S., Li, Z., Liu, L., Guo, Y., Huang, Y., Bowen, A.D., Liu, M., Wang, M., Yu, J., et al.
632 (2022). Alarming antibody evasion properties of rising SARS-CoV-2 BQ and XBB subvariants. Cell.
633 https://doi.org/10.1016/j.cell.2022.12.018.

634 13. Westendorf, K., Žentelis, S., Wang, L., Foster, D., Vaillancourt, P., Wiggin, M., Lovett, E., van der Lee, R.,
635 Hendle, J., Pustilnik, A., et al. (2022). LY-CoV1404 (bebtelovimab) potently neutralizes SARS-CoV-2
636 variants. Cell Rep. *39*. https://doi.org/10.1016/j.celrep.2022.110812.

637 14. Taylor, P.C., Adams, A.C., Hufford, M.M., de la Torre, I., Winthrop, K., and Gottlieb, R.L. (2021).
638 Neutralizing monoclonal antibodies for treatment of COVID-19. Nat. Rev. Immunol. *21*, 382–393.
639 https://doi.org/10.1038/s41577-021-00542-x.

640 15. Li, G., Hilgenfeld, R., Whitley, R., and De Clercq, E. (2023). Therapeutic strategies for COVID-19: progress
641 and lessons learned. Nat. Rev. Drug Discov. *22*, 449–475. https://doi.org/10.1038/s41573-023-00672-y.

642 16. Gliga, S., Lübke, N., Killer, A., Gruell, H., Walker, A., Dilthey, A.T., Thielen, A., Lohr, C., Flaßhove, C., Krieg,
643 S., et al. (2022). Rapid Selection of Sotrovimab Escape Variants in Severe Acute Respiratory Syndrome
644 Coronavirus 2 (SARS-CoV-2) Omicron-Infected Immunocompromised Patients. Clinical Infectious
645 Diseases, 5–6. https://doi.org/10.1093/cid/ciac802.

646 17. Planas, D., Bruel, T., Staropoli, I., Guivel-Benhassine, F., Porrot, F., Maes, P., Grzelak, L., Prot, M.,
647 Mougari, S., Planchais, C., et al. (2023). Resistance of Omicron subvariants BA.2.75.2, BA.4.6, and BQ.1.1
648 to neutralizing antibodies. Nat. Commun. *14*, 1–11. https://doi.org/10.1038/s41467-023-36561-6.

649 18. Cao, Y., Jian, F., Zhang, Z., Yisimayi, A., Hao, X., Bao, L., Yuan, F., Yu, Y., Du, S., Wang, J., et al. (2022).
650 Rational identification of potent and broad sarbecovirus-neutralizing antibody cocktails from SARS
651 convalescents. Cell Rep. *41*, 111845. https://doi.org/10.1016/j.celrep.2022.111845.

652 19. Rosen, L.E., Tortorici, M.A., De Marco, A., Pinto, D., Foreman, W.B., Taylor, A.L., Park, Y.J., Bohan, D.,
653 Rietz, T., Errico, J.M., et al. (2024). A potent pan-sarbecovirus neutralizing antibody resilient to epitope
654 diversification. Cell, 1–18. https://doi.org/10.1016/j.cell.2024.09.026.

655 20. Ellis, R., and Weiss, A. (2025). Human vaccines and immunotherapeutics: News February 2025. Hum.
656 Vaccin. Immunother. *21*, 4–5. https://doi.org/10.1080/21645515.2025.2482479.

657 21. Mellis, I.A., Wu, M., Hong, H., Tzang, C.-C., Bowen, A., Wang, Q., Gherasim, C., Pierce, V.M., Shah, J.G.,
658 Purpura, L.J., et al. (2025). Antibody evasion and receptor binding of SARS-CoV-2 LP.8.1.1, NB.1.8.1,
659 XFG, and related subvariants. Cell Rep. *44*. https://doi.org/10.1016/j.celrep.2025.116440.

660 22. Anand, S.P., Prévost, J., Nayrac, M., Beaudoin-Bussières, G., Benlarbi, M., Gasser, R., Brassard, N.,
661 Laumaea, A., Gong, S.Y., Bourassa, C., et al. (2021). Longitudinal analysis of humoral immunity against
662 SARS-CoV-2 Spike in convalescent individuals up to 8 months post-symptom onset. Cell Rep. Med. *2*.
663 https://doi.org/10.1016/j.xcrm.2021.100290.

664 23. Zohar, T., Loos, C., Fischinger, S., Atyeo, C., Wang, C., Slein, M.D., Burke, J., Yu, J., Feldman, J., Hauser,
665 B.M., et al. (2020). Compromised Humoral Functional Evolution Tracks with SARS-CoV-2 Mortality. Cell
666 *183*, 1508-1519.e12. https://doi.org/10.1016/j.cell.2020.10.052.

667 24. Izadi, A., and Nordenfelt, P. (2024). Protective non-neutralizing SARS-CoV-2 monoclonal antibodies.
668 Trends Immunol. *xx*, 1–16. https://doi.org/10.1016/j.it.2024.06.003.

669 25. Kaplonek, P., Cizmeci, D., Fischinger, S., Collier, A.R., Suscovich, T., Linde, C., Broge, T., Mann, C.,
670 Amanat, F., Dayal, D., et al. (2022). mRNA-1273 and BNT162b2 COVID-19 vaccines elicit antibodies with
671 differences in Fc-mediated effector functions. Sci. Transl. Med. *14*, 1–12.
672 https://doi.org/10.1126/scitranslmed.abm2311.

673 26. Hederman, A.P., Natarajan, H., Heyndrickx, L., Ariën, K.K., Wiener, J.A., Wright, P.F., Bloch, E.M., Tobian,
674 A.A.R., Redd, A.D., Blankson, J.N., et al. (2023). SARS-CoV-2 vaccination elicits broad and potent antibody
675 effector functions to variants of concern in vulnerable populations. Nat. Commun. *14*, 1–11.
676 https://doi.org/10.1038/s41467-023-40960-0.

677 27. Ullah, I., Beaudoin-Bussières, G., Symmes, K., Cloutier, M., Ducas, E., Tauzin, A., Laumaea, A., Grunst,
678 M.W., Dionne, K., Richard, J., et al. (2023). The Fc-effector function of COVID-19 convalescent plasma
679 contributes to SARS-CoV-2 treatment efficacy in mice. Cell Rep. Med. *4*.
680 https://doi.org/10.1016/j.xcrm.2022.100893.

681 28. Schäfer, A., Muecksch, F., Lorenzi, J.C.C., Leist, S.R., Cipolla, M., Bournazos, S., Schmidt, F., Maison,
682 R.M., Gazumyan, A., Martinez, D.R., et al. (2021). Antibody potency, effector function, and combinations in
683 protection and therapy for SARS-CoV-2 infection in vivo. Journal of Experimental Medicine *218*.
684 https://doi.org/10.1084/jem.20201993.

685 29. Dufloo, J., Grzelak, L., Staropoli, I., Madec, Y., Tondeur, L., Anna, F., Pelleau, S., Wiedemann, A.,
686 Planchais, C., Buchrieser, J., et al. (2021). Asymptomatic and symptomatic SARS-CoV-2 infections elicit
687 polyfunctional antibodies. Cell Rep. Med. *2*, 100275. https://doi.org/10.1016/j.xcrm.2021.100275.

688 30. Beaudoin-Bussières, G., and Finzi, A. (2024). Deciphering Fc-effector functions against SARS-CoV-2.
689 Preprint, https://doi.org/10.1016/j.tim.2024.01.005 https://doi.org/10.1016/j.tim.2024.01.005.

690 31. Zhang, A., Stacey, H.D., D'Agostino, M.R., Tugg, Y., Marzok, A., and Miller, M.S. (2023). Beyond
691 neutralization: Fc-dependent antibody effector functions in SARS-CoV-2 infection. Nat. Rev. Immunol. *23*,
692 381–396. https://doi.org/10.1038/s41577-022-00813-1.

693 32. Izadi, A., and Nordenfelt, P. (2024). Protective non-neutralizing SARS-CoV-2 monoclonal antibodies.
694 Trends Immunol. *45*, 609–624. https://doi.org/10.1016/j.it.2024.06.003.

695 33. Bruel, T., Vrignaud, L.L., Porrot, F., Staropoli, I., Planas, D., Guivel-Benhassine, F., Puech, J., Prot, M.,
696 Munier, S., Bolland, W.H., et al. (2023). Sotrovimab therapy elicits antiviral activities against Omicron
697 BQ.1.1 and XBB.1.5 in sera of immunocompromised patients. Preprint,
698 https://doi.org/10.1016/j.medj.2023.07.007 https://doi.org/10.1016/j.medj.2023.07.007.

34. Addetia, A., Piccoli, L., Case, J.B., Park, Y.J., Beltramello, M., Guarino, B., Dang, H., de Melo, G.D., Pinto, D., Sprouse, K., et al. (2023). Neutralization, effector function and immune imprinting of Omicron variants. Nature *621*. https://doi.org/10.1038/s41586-023-06487-6.

35. Bianchini, F., Crivelli, V., Abernathy, M.E., Guerra, C., Palus, M., Muri, J., Marcotte, H., Piralla, A., Pedotti, M., De Gasparo, R., et al. (2023). Human neutralizing antibodies to cold linear epitopes and subdomain 1 of the SARS-CoV-2 spike glycoprotein. Sci. Immunol. *8*, 1–18. https://doi.org/10.1126/sciimmunol.ade0958.

36. Sun, X., Yi, C., Zhu, Y., Ding, L., Xia, S., Chen, X., Liu, M., Gu, C., Lu, X., Fu, Y., et al. (2022). Neutralization mechanism of a human antibody with pan-coronavirus reactivity including SARS-CoV-2. Nat. Microbiol. *7*, 1063–1074. https://doi.org/10.1038/s41564-022-01155-3.

37. Low, J.S., Jerak, J., Tortorici, M.A., McCallum, M., Pinto, D., Cassotta, A., Foglierini, M., Mele, F., Abdelnabi, R., Weynand, B., et al. (2022). ACE2-binding exposes the SARS-CoV-2 fusion peptide to broadly neutralizing coronavirus antibodies. Science (1979). *377*, 735–742. https://doi.org/10.1126/science.abq2679.

38. Planchais, C., Fernández, I., Bruel, T., de Melo, G.D., Prot, M., Beretta, M., Guardado-Calvo, P., Dufloo, J., Molinos-Albert, L.M., Backovic, M., et al. (2022). Potent human broadly SARS-CoV-2–neutralizing IgA and IgG antibodies effective against Omicron BA.1 and BA.2. Preprint, https://doi.org/10.1084/jem.20220638 https://doi.org/10.1084/jem.20220638.

39. Planchais, C., Fernández, I., Bruel, T., de Melo, G.D., Prot, M., Beretta, M., Guardado-Calvo, P., Dufloo, J., Molinos-Albert, L.M., Backovic, M., et al. (2022). Potent human broadly SARS-CoV-2–neutralizing IgA and IgG antibodies effective against Omicron BA.1 and BA.2. Journal of Experimental Medicine *219*. https://doi.org/10.1084/jem.20220638.

40. Hansen, J., Baum, A., Pascal, K.E., Russo, V., Giordano, S., Wloga, E., Fulton, B.O., Yan, Y., Koon, K., Patel, K., et al. (2020). Studies in humanized mice and convalescent humans yield a SARS-CoV-2 antibody cocktail. Science (1979). *369*, 1010–1014. https://doi.org/10.1126/science.abd0827.

41. Shi, Y., Wang, Y., Shao, C., Huang, J., Gan, J., Huang, X., Bucci, E., Piacentini, M., Ippolito, G., and Melino, G. (2020). COVID-19 infection: the perspectives on immune responses. Cell Death Differ. *27*, 1451–1454. https://doi.org/10.1038/s41418-020-0530-3.

42. Jones, B.E., Brown-Augsburger, P.L., Corbett, K.S., Westendorf, K., Davies, J., Cujec, T.P., Wiethoff, C.M., Blackbourne, J.L., Heinz, B.A., Foster, D., et al. (2021). The neutralizing antibody, LY-CoV555, protects against SARS-CoV-2 infection in nonhuman primates. Sci. Transl. Med. *13*, 1–18. https://doi.org/10.1126/scitranslmed.abf1906.

43. Kim, C., Ryu, D.K., Lee, J., Kim, Y. Il, Seo, J.M., Kim, Y.G., Jeong, J.H., Kim, M., Kim, J.I., Kim, P., et al. (2021). A therapeutic neutralizing antibody targeting receptor binding domain of SARS-CoV-2 spike protein. Nat. Commun. *12*, 1–10. https://doi.org/10.1038/s41467-020-20602-5.

44. Zost, S.J., Gilchuk, P., Case, J.B., Binshtein, E., Chen, R.E., Nkolola, J.P., Schäfer, A., Reidy, J.X., Trivette, A., Nargi, R.S., et al. (2020). Potently neutralizing and protective human antibodies against SARS-CoV-2. Nature *584*, 443–449. https://doi.org/10.1038/s41586-020-2548-6.

45. Garrett Rappazzo, C., Tse, L. V., Kaku, C.I., Wrapp, D., Sakharkar, M., Huang, D., Deveau, L.M., Yockachonis, T.J., Herbert, A.S., Battles, M.B., et al. (2021). Broad and potent activity against SARS-like viruses by an engineered human monoclonal antibody. Science (1979). *371*, 823–829. https://doi.org/10.1126/science.abf4830.

46. Pinto, D., Park, Y.J., Beltramello, M., Walls, A.C., Tortorici, M.A., Bianchi, S., Jaconi, S., Culap, K., Zatta, F., De Marco, A., et al. (2020). Cross-neutralization of SARS-CoV-2 by a human monoclonal SARS-CoV antibody. Nature *583*, 290–295. https://doi.org/10.1038/s41586-020-2349-y.

47. Buchrieser, J., Dufloo, J., Hubert, M., Monel, B., Planas, D., Rajah, M.M., Planchais, C., Porrot, F., Guivel-Benhassine, F., Van der Werf, S., et al. (2020). Syncytia formation by SARS-CoV-2-infected cells. EMBO J. *39*, 1–12. https://doi.org/10.15252/embj.2020106267.

48. Planchais, C., Fernández, I., Bruel, T., de Melo, G.D., Prot, M., Beretta, M., Guardado-Calvo, P., Dufloo, J., Molinos-Albert, L.M., Backovic, M., et al. (2022). Potent human broadly SARS-CoV-2–neutralizing IgA and IgG antibodies effective against Omicron BA.1 and BA.2. Journal of Experimental Medicine *219*. https://doi.org/10.1084/jem.20220638.

750 49. Sun, X., Yi, C., Zhu, Y., Ding, L., Xia, S., Chen, X., Liu, M., Gu, C., Lu, X., Fu, Y., et al. (2022). Neutralization
751 mechanism of a human antibody with pan-coronavirus reactivity including SARS-CoV-2. Nat. Microbiol. *7*,
752 1063–1074. https://doi.org/10.1038/s41564-022-01155-3.

753 50. Low, J.S., Jerak, J., Tortorici, M.A., McCallum, M., Pinto, D., Cassotta, A., Foglierini, M., Mele, F.,
754 Abdelnabi, R., Weynand, B., et al. (2022). ACE2-binding exposes the SARS-CoV-2 fusion peptide to
755 broadly neutralizing coronavirus antibodies. Science (1979). *377*, 735–742.
756 https://doi.org/10.1126/science.abq2679.

757 51. Bianchini, F., Crivelli, V., Abernathy, M.E., Guerra, C., Palus, M., Muri, J., Marcotte, H., Piralla, A., Pedotti,
758 M., De Gasparo, R., et al. (2023). Human neutralizing antibodies to cold linear epitopes and subdomain 1
759 of the SARS-CoV-2 spike glycoprotein. Sci. Immunol. *8*, 1–18. https://doi.org/10.1126/sciimmunol.ade0958.

760 52. Mast, F.D., Fridy, P.C., Ketaren, N.E., Wang, J., Jacobs, E.Y., Olivier, J.P., Sanyal, T., Molloy, K.R.,
761 Schmidt, F., Rutkowska, M., et al. (2021). Highly synergistic combinations of nanobodies that target SARS-
762 CoV-2 and are resistant to escape. Elife *10*. https://doi.org/10.7554/eLife.73027.

763 53. Piepenbrink, M.S., Park, J.G., Deshpande, A., Loos, A., Ye, C., Basu, M., Sarkar, S., Khalil, A.M., Chauvin,
764 D., Woo, J., et al. (2022). Potent universal beta-coronavirus therapeutic activity mediated by direct
765 respiratory administration of a Spike S2 domain-specific human neutralizing monoclonal antibody. PLoS
766 Pathog. *18*. https://doi.org/10.1371/journal.ppat.1010691.

767 54. Dacon, C., Tucker, C., Peng, L., Lee, C.C.D., Lin, T.H., Yuan, M., Cong, Y., Wang, L., Purser, L., Williams,
768 J.K., et al. (2022). Broadly neutralizing antibodies target the coronavirus fusion peptide. Science (1979).
769 *377*, 728–735. https://doi.org/10.1126/science.abq3773.

770 55. Shi, R., Shan, C., Duan, X., Chen, Z., Liu, P., Song, J., Song, T., Bi, X., Han, C., Wu, L., et al. (2020). A
771 human neutralizing antibody targets the receptor-binding site of SARS-CoV-2. Nature *584*, 120–124.
772 https://doi.org/10.1038/s41586-020-2381-y.

773 56. Ullah, I., Beaudoin-Bussières, G., Symmes, K., Cloutier, M., Ducas, E., Tauzin, A., Laumaea, A., Grunst,
774 M.W., Dionne, K., Richard, J., et al. (2023). The Fc-effector function of COVID-19 convalescent plasma
775 contributes to SARS-CoV-2 treatment efficacy in mice. Cell Rep. Med. *4*, 100893.
776 https://doi.org/10.1016/j.xcrm.2022.100893.

777 57. Edgar, J.E., and Bournazos, S. (2024). Fc-FcγR interactions during infections: From neutralizing antibodies
778 to antibody-dependent enhancement. Preprint, https://doi.org/10.1111/imr.13393
779 https://doi.org/10.1111/imr.13393.

780 58. Case, J.B., Jain, S., Suthar, M.S., and Diamond, M.S. (2025). SARS-CoV-2: The Interplay Between
781 Evolution and Host Immunity. Preprint, https://doi.org/10.1146/annurev-immunol-083122-043054
782 https://doi.org/10.1146/annurev-immunol-083122-043054.

783 59. Cox, M., Peacock, T.P., Harvey, W.T., Hughes, J., Wright, D.W., Willett, B.J., Thomson, E., Gupta, R.K.,
784 Peacock, S.J., Robertson, D.L., et al. (2023). SARS-CoV-2 variant evasion of monoclonal antibodies based
785 on in vitro studies. Nat. Rev. Microbiol. *21*, 112–124. https://doi.org/10.1038/s41579-022-00809-7.

786 60. Planchais, C., Fernández, I., Chalopin, B., Bruel, T., Rosenbaum, P., Beretta, M., Dimitrov, J.D., Conquet,
787 L., Donati, F., Prot, M., et al. (2024). Broad sarbecovirus neutralization by combined memory B cell
788 antibodies to ancestral SARS-CoV-2. iScience *27*, 110354.
789 https://doi.org/https://doi.org/10.1016/j.isci.2024.110354.

790 61. Paciello, I., Maccari, G., Pantano, E., Andreano, E., and Rappuoli, R. (2024). High-resolution map of the Fc
791 functions mediated by COVID-19- neutralizing antibodies. Proc. Natl. Acad. Sci. U. S. A. *121*.
792 https://doi.org/10.1073/pnas.2314730121.

793 62. Clark, J.J., Hoxie, I., Adelsberg, D.C., Sapse, I.A., Andreata-Santos, R., Yong, J.S., Amanat, F., Tcheou,
794 J., Raskin, A., Singh, G., et al. (2024). Protective effect and molecular mechanisms of human non-
795 neutralizing cross-reactive spike antibodies elicited by SARS-CoV-2 mRNA vaccination. Cell Rep. *43*,
796 114922. https://doi.org/10.1016/j.celrep.2024.114922.

797 63. Winkler, E.S., Gilchuk, P., Yu, J., Bailey, A.L., Chen, R.E., Chong, Z., Zost, S.J., Jang, H., Huang, Y., Allen,
798 J.D., et al. (2021). Human neutralizing antibodies against SARS-CoV-2 require intact Fc effector functions
799 for optimal therapeutic protection. Preprint, https://doi.org/10.1016/j.cell.2021.02.026
800 https://doi.org/10.1016/j.cell.2021.02.026.

64. Tan, T.J.C., Verma, A.K., Odle, A., Lei, R., Meyerholz, D.K., Matreyek, K.A., Perlman, S., Wong, L.-Y.R., and Wu, N.C. (2024). Evidence of antigenic drift in the fusion machinery core of SARS-CoV-2 spike. Proceedings of the National Academy of Sciences *121*. https://doi.org/10.1073/pnas.2317222121.

65. Pierre, C.N., Adams, L.E., Higgins, J.S., Anasti, K., Goodman, D., Mielke, D., Stanfield-Oakley, S., Powers, J.M., Li, D., Rountree, W., et al. (2024). Non-neutralizing SARS-CoV-2 N-terminal domain antibodies protect mice against severe disease using Fc-mediated effector functions. PLoS Pathog. *20*. https://doi.org/10.1371/journal.ppat.1011569.

66. Cao, Y., Yisimayi, A., Jian, F., Song, W., Xiao, T., Wang, L., Du, S., Wang, J., Li, Q., Chen, X., et al. (2022). BA.2.12.1, BA.4 and BA.5 escape antibodies elicited by Omicron infection. Nature *608*, 593–602. https://doi.org/10.1038/s41586-022-04980-y.

67. Cao, Y., Jian, F., Wang, J., Yu, Y., Song, W., Yisimayi, A., Wang, J., An, R., Chen, X., Zhang, N., et al. (2022). Imprinted SARS-CoV-2 humoral immunity induces convergent Omicron RBD evolution. Nature. https://doi.org/10.1038/s41586-022-05644-7.

68. Cao, Y., Wang, J., Jian, F., Xiao, T., Song, W., Yisimayi, A., Huang, W., Li, Q., Wang, P., An, R., et al. (2022). Omicron escapes the majority of existing SARS-CoV-2 neutralizing antibodies. Nature *602*. https://doi.org/10.1038/s41586-021-04385-3.

69. Planas, D., Saunders, N., Maes, P., Guivel-Benhassine, F., Planchais, C., Buchrieser, J., Bolland, W.-H., Porrot, F., Staropoli, I., Lemoine, F., et al. (2022). Considerable escape of SARS-CoV-2 Omicron to antibody neutralization. Nature *602*, 671–675. https://doi.org/10.1038/s41586-021-04389-z.

70. Kaplonek, P., Fischinger, S., Cizmeci, D., Bartsch, Y.C., Kang, J., Burke, J.S., Shin, S.A., Dayal, D., Martin, P., Mann, C., et al. (2022). mRNA-1273 vaccine-induced antibodies maintain Fc effector functions across SARS-CoV-2 variants of concern. Immunity *55*. https://doi.org/10.1016/j.immuni.2022.01.001.

71. Manamela, N.P., Motsoeneng, B.M., Spencer, H., Hermanus, T., Mzindle, N., Ayres, F., Makhado, Z., Serage, R., Gray, G.G., Bekker, L.G., et al. (2025). SARS-CoV-2 vaccines elicit differential Fc effector functions. iScience *28*. https://doi.org/10.1016/j.isci.2025.113084.

72. Bartsch, Y.C., St. Denis, K.J., Kaplonek, P., Kang, J., Lam, E.C., Burns, M.D., Farkas, E.J., Davis, J.P., Boribong, B.P., Edlow, A.G., et al. (2022). SARS-CoV-2 mRNA vaccination elicits robust antibody responses in children. Sci. Transl. Med. *14*. https://doi.org/10.1126/scitranslmed.abn9237.

73. Bartsch, Y.C., Cizmeci, D., Kang, J., Gao, H., Shi, W., Chandrashekar, A., Collier, A. ris Y., Chen, B., Barouch, D.H., and Alter, G. (2023). Selective SARS-CoV2 BA.2 escape of antibody Fc/Fc-receptor interactions. iScience *26*. https://doi.org/10.1016/j.isci.2023.106582.

74. Planas, D., Veyer, D., Baidaliuk, A., Staropoli, I., Guivel-Benhassine, F., Rajah, M.M., Planchais, C., Porrot, F., Robillard, N., Puech, J., et al. (2021). Reduced sensitivity of SARS-CoV-2 variant Delta to antibody neutralization. Nature *596*, 276–280. https://doi.org/10.1038/s41586-021-03777-9.

75. Planas, D., Bruel, T., Grzelak, L., Guivel-Benhassine, F., Staropoli, I., Porrot, F., Planchais, C., Buchrieser, J., Rajah, M.M., Bishop, E., et al. (2021). Sensitivity of infectious SARS-CoV-2 B.1.1.7 and B.1.351 variants to neutralizing antibodies. Nat. Med. *27*, 917–924. https://doi.org/10.1038/s41591-021-01318-5.

76. Grzelak, L., Temmam, S., Planchais, C., Demeret, C., Tondeur, L., Huon, C., Guivel-Benhassine, F., Staropoli, I., Chazal, M., Dufloo, J., et al. (2020). A comparison of four serological assays for detecting anti–SARS-CoV-2 antibodies in human serum samples from different populations. Sci. Transl. Med. *12*, 1–13. https://doi.org/10.1126/scitranslmed.abc3103.

77. Planas, D., Bruel, T., Staropoli, I., Guivel-Benhassine, F., Porrot, F., Maes, P., Grzelak, L., Prot, M., Mougari, S., Planchais, C., et al. (2023). Resistance of Omicron subvariants BA.2.75.2, BA.4.6, and BQ.1.1 to neutralizing antibodies. Nat. Commun. *14*, 824. https://doi.org/10.1038/s41467-023-36561-6.

78. Planas, D., Staropoli, I., Michel, V., Lemoine, F., Donati, F., Prot, M., Porrot, F., Guivel-Benhassine, F., Jeyarajah, B., Brisebarre, A., et al. (2024). Distinct evolution of SARS-CoV-2 Omicron XBB and BA.2.86/JN.1 lineages combining increased fitness and antibody evasion. Nat. Commun. *15*, 2254. https://doi.org/10.1038/s41467-024-46490-7.

79. Betton, M., Livrozet, M., Planas, D., Fayol, A., Monel, B., Védie, B., Bruel, T., Tartour, E., Robillard, N., Manuguerra, J.C., et al. (2021). Sera Neutralizing Activities Against Severe Acute Respiratory Syndrome Coronavirus 2 and Multiple Variants 6 Months After Hospitalization for Coronavirus Disease 2019. Clinical Infectious Diseases *73*, E1337–E1344. https://doi.org/10.1093/cid/ciab308.

80. Lorin, V., and Mouquet, H. (2015). Efficient generation of human IgA monoclonal antibodies. J. Immunol. Methods *422*, 102–110. https://doi.org/10.1016/j.jim.2015.04.010.

81. Wardemann, H., Yurasov, S., Schaefer, A., Young, J.W., Meffre, E., and Nussenzweig, M.C. (2003). Predominant autoantibody production by early human B cell precursors. Science (1979). *301*, 1374–1377. https://doi.org/10.1126/science.1086907.

82. Prigent, J., Lorin, V., Kök, A., Hieu, T., Bourgeau, S., and Mouquet, H. (2016). Scarcity of autoreactive human blood IgA+ memory B cells. Eur. J. Immunol. *46*, 2340–2351. https://doi.org/10.1002/eji.201646446.

83. Tiller, T., Meffre, E., Yurasov, S., Tsuiji, M., Nussenzweig, M.C., and Wardemann, H. (2008). Efficient generation of monoclonal antibodies from single human B cells by single cell RT-PCR and expression vector cloning. J. Immunol. Methods *329*, 112–124. https://doi.org/10.1016/j.jim.2007.09.017.

84. Dufloo, J., Grzelak, L., Staropoli, I., Madec, Y., Tondeur, L., Anna, F., Pelleau, S., Wiedemann, A., Planchais, C., Buchrieser, J., et al. (2021). Asymptomatic and symptomatic SARS-CoV-2 infections elicit polyfunctional antibodies. Cell Rep. Med. *2*. https://doi.org/10.1016/j.xcrm.2021.100275.

French COVID Cohort Study Group

Marie Bartoli[1], Alpha Diallo[1], Soizic Le Mestre[1], Christelle Paul[1], Ventzislava Petrov-Sanchez[1], Yazdan Yazdanpanah[1], Cécile Ficko[2], Catherine Chirouze[3], Claire Andrejak[4], Denis Malvy[5], François Goehringer[6], Patrick Rossignol[6], Tristan Gigante[6], Morgane Gilg[6], Bénédicte Rossignol[6], Manuel Etienne[7], Marine Beluze[8], Delphine Bachelet[9], Krishna Bhavsar[9], Lila Bouadma[9], Minerva Cervantes-Gonzalez[9], Anissa Chair[9], Charlotte Charpentier[9], Léo Chenard[9], Camille Couffignal[9], Marie-Pierre Debray[9], Diane Descamps[9], Xavier Duval[9], Philippine Eloy[9], Marina Esposito-Farese[9], Aline-Marie Florence[9], Jade Ghosn[9], Isabelle Hoffmann[9], Ouifiya Kafif[9], Antoine Khalil[9], Nadhem Lafhej[9], Cédric Laouénan[9], Samira Laribi[9], Minh Le[9], Quentin Le Hingrat[9], Sophie Letrou[9], France Mentré[9], Gilles Peytavin[9], Valentine Piquard[9], Carine Roy[9], Marion Schneider[9], Richa Su[9], Coralie Tardivon[9], Jean-François Timsit[9], Sarah Tubiana[9], Benoît Visseaux[9], Dominique Deplanque[10], Jean-Sébastien Hulot[11], Jean-Luc Diehl[11], Olivier Picone[12], François Angoulvant[13], Amal Abrous[14], Sandrine Couffin-Cadiergues[14], Fernanda Dias Da Silva[14], Hélène Esperou[14], Ikram Houas[14], Salma Jaafoura[14], Aurélie Papadopoulos[14], Alexandre Gaymard[15], Bruno Lina[15], Manuel Rosa-Calatrava[15], Céline Dorival[16], Jérémie Guedj[17], Guillaume Lingas[17], Nadège Neant[17], Laurent Abel[18], Victoria Manda[19], Sylvie Behillil[20], Vincent Enouf[20], Yves Levy[21] and Aurélie Wiedemann[21]

[1]Agence Nationale de Recherches sur le Sida et les Hépatites virales-Maladies Infectieuses Émergentes (ANRS-MIE), 75015 Paris, France

[2]Hôpital d'Instruction des Armées Bégin, Service des Maladies Infectieuses et Tropicales, 94160 Saint-Mandé, France

[3]Centre Hospitalier Régional Universitaire Jean Minjoz, 25056 Besançon, France

[4]Centre Hospitalier Universitaire, 80080 Amiens, France

[5]Centre Hospitalier Universitaire, 33000 Bordeaux, France

[6]Centre Hospitalier Régional Universitaire, 54000 Nancy, France

[7]Centre Hospitalier Universitaire, 76000 Rouen, France

[8]French Clinical Research Infrastructure Network (F-CRIN), 75013 Paris, France

[9]Hôpital Bichat, AP-HP, 75018 Paris, France

[10]Hopital Calmette, 59000 Lille, France

[11]Hôpital Européen Georges Pompidou, AP-HP, 75015 Paris, France

[12]Hôpital Louis Mourier, 92700 Colombes, France

[13]Hôpital Necker, AP-HP, 75015 Paris, France

[14]Institut National de la Santé et de la Recherche Médicale (INSERM), 75013 Paris, France

[15]INSERM UMR 1111, 69007 Lyon, France

[16]INSERM UMR 1136, 75646 Paris, France

[17]INSERM UMR 1137, 75018 Paris, France

[18]INSERM UMR 1163, 75015 Paris, France

[19]Hopital Lariboisière, AP-HP, 75010 Paris, France

[20]Institut Pasteur, Université Paris Cité, Molecular Genetics of RNA Viruses, F-75015 Paris, France
[21]Institut de Recherche Vaccinale (VRI), INSERM UMR 955, 94000 Créteil, France

CORSER Study Group

Laurence Arowas[1], Blanca Liliana Perlaza[1], Louise Perrin de Facci[1], Sophie Chaouche[1], Linda Sangari[1], Charlotte Renaudat[1], Sandrine Fernandes Pellerin[2], Cassandre van Platen[2], Nathalie Jolly[2], Lucie Kuhmel[3], Valentine Garaud[3], Hantaniaina Rafanoson[3], Soazic Gardais[4], Nathalie de Parseval[5], Claire Dugast[5], Caroline Jannet[5], Sandrine Ropars[5], Fanny Momboisse[5], Isabelle Porteret[5], Isabelle Cailleau[6], Bruno Hoen[6], Laura Tondeur[7], Camille Besombes[7], Arnaud Fontanet[7]

[1]ICAReB platform (Clinical Investigation & Access to Research Bioresources) of the Center for Translational Science, Institut Pasteur, F-75015 Paris, France

[2]Center for Translational Sciences, Institut Pasteur, F-75015 Paris, France

[3]Medical Center of the Institut Pasteur, Institut Pasteur, F-75015 Paris, France

[4]G5 Infectious Disease Epidemiology, Institut Pasteur, F-75015 Paris, France

[5]Institut Pasteur, F-75015 Paris, France

[6]Direction de la recherche médicale, Institut Pasteur, F-75015 Paris, France

[7]Emerging Diseases Epidemiology Unit, Institut Pasteur, F-75015 Paris, France

Figure 1

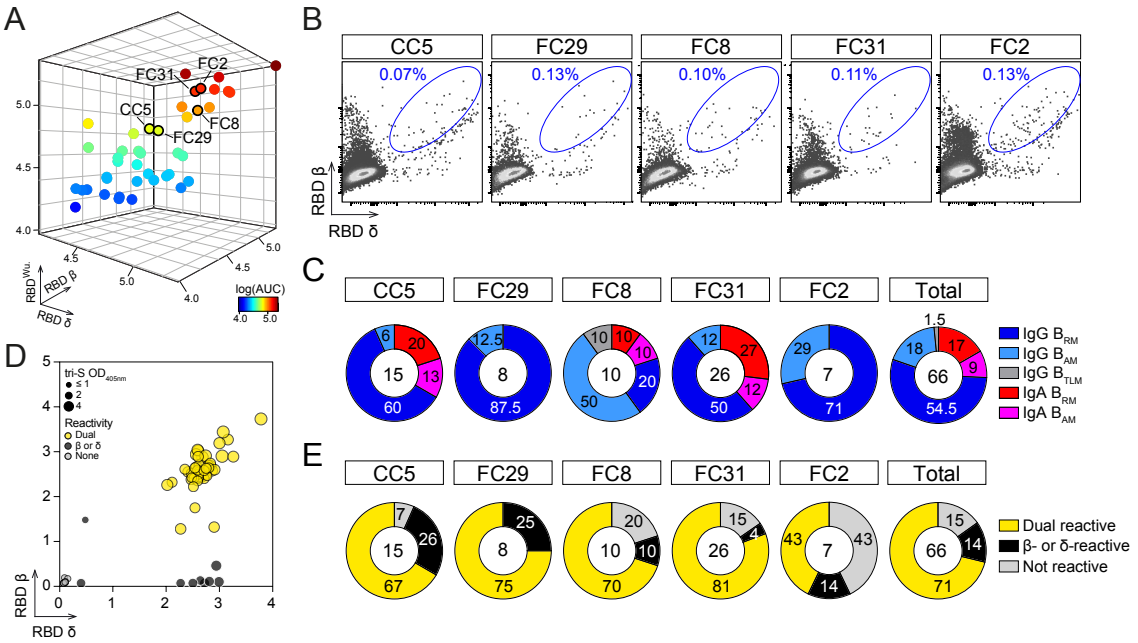
A
FC31
FC2
CC5
FC8
FC29
5.0
4.5
4.0
RBD Wu
RBD β
RBD δ
log(AUC)
B
CC5
FC29
FC8
FC31
FC2
0.07%
0.13%
0.10%
0.11%
0.13%
RBD β
RBD δ
C
CC5
FC29
FC8
FC31
FC2
Total
IgG B RM
IgG B AM
IgG B TLM
IgA B RM
IgA B AM
D
tri-S OD 405nm
≤ 1
2
4
Reactivity
Dual
β or δ
None
RBD β
RBD δ
E
CC5
FC29
FC8
FC31
FC2
Total
Dual reactive
β- or δ-reactive
Not reactive

Figure 2

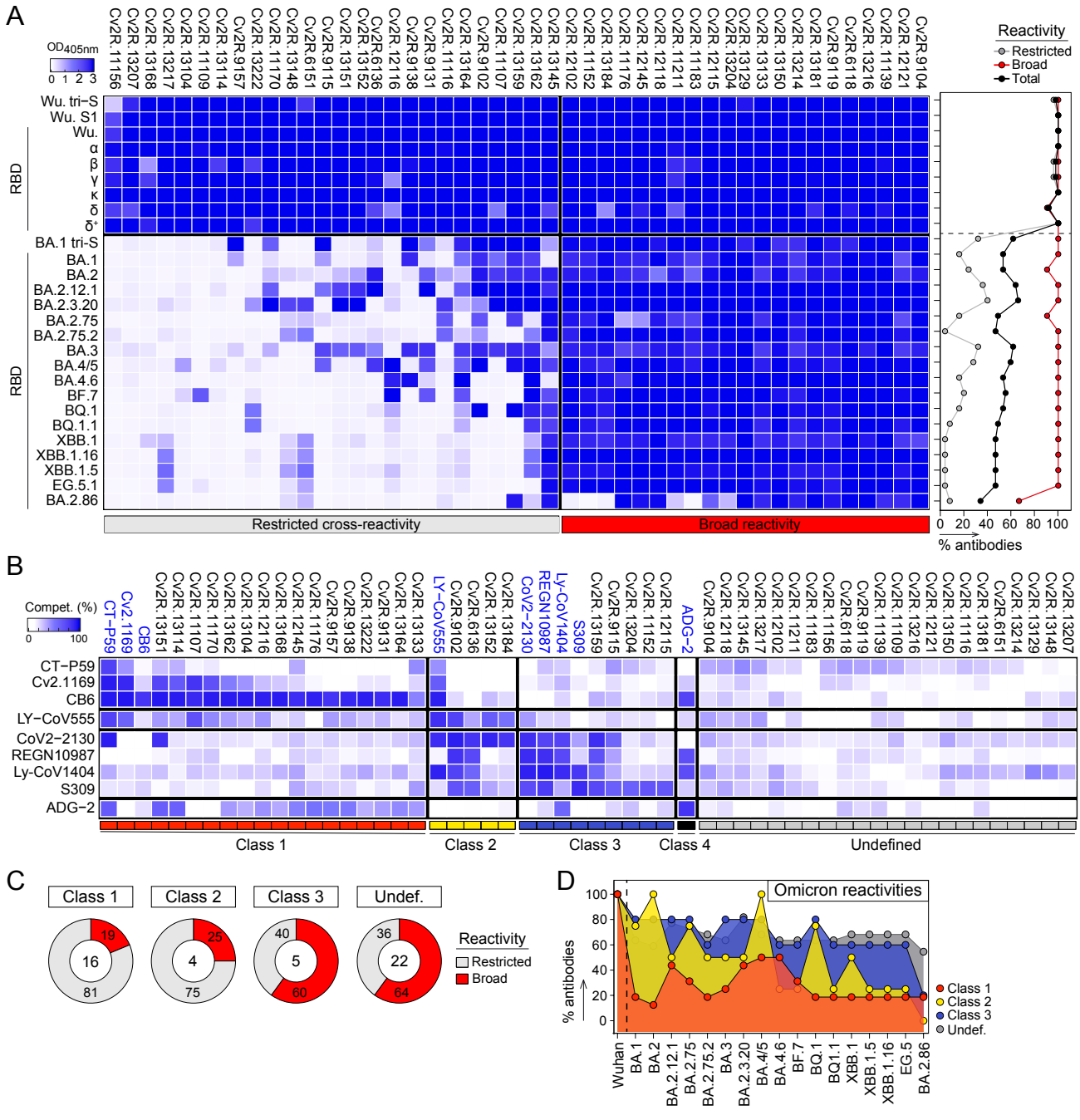
A
OD405nm
0 1 2 3
Cv2R.11156 Cv2R.13207 Cv2R.13168 Cv2R.13217 Cv2R.13104 Cv2R.11109 Cv2R.13114 Cv2R.9157 Cv2R.13222 Cv2R.11170 Cv2R.13148 Cv2R.6151 Cv2R.9115 Cv2R.13151 Cv2R.13152 Cv2R.6136 Cv2R.12116 Cv2R.9138 Cv2R.9131 Cv2R.11116 Cv2R.13164 Cv2R.9102 Cv2R.11107 Cv2R.13159 Cv2R.13162 Cv2R.13145 Cv2R.12102 Cv2R.11152 Cv2R.13184 Cv2R.11176 Cv2R.12145 Cv2R.12118 Cv2R.11211 Cv2R.11183 Cv2R.12115 Cv2R.13204 Cv2R.13129 Cv2R.13133 Cv2R.13150 Cv2R.13214 Cv2R.13181 Cv2R.9119 Cv2R.6118 Cv2R.13216 Cv2R.11139 Cv2R.12121 Cv2R.9104
RBD
Wu. tri-S
Wu. S1
Wu.
α
β
γ
κ
δ
δ+
BA.1 tri-S
BA.1
BA.2
BA.2.12.1
BA.2.3.20
BA.2.75
BA.2.75.2
BA.3
BA.4/5
BA.4.6
BF.7
BQ.1
BQ.1.1
XBB.1
XBB.1.16
XBB.1.5
EG.5.1
BA.2.86
Restricted cross-reactivity
Broad reactivity
Reactivity
Restricted
Broad
Total
0 20 40 60 80 100
% antibodies
B
Compet. (%)
0 100
CT-P59 Cv2.1169 CB6 LY-CoV555 CoV2-2130 REGN10987 Ly-CoV1404 S309 ADG-2
Class 1
Class 2
Class 3
Class 4
Undefined
C
Class 1
Class 2
Class 3
Undef.
16 19 81
4 25 75
5 40 60
22 36 64
Reactivity
Restricted
Broad
D
Omicron reactivities
% antibodies
0 20 40 60 80 100
Wuhan BA.1 BA.2 BA.2.12.1 BA.2.75 BA.2.75.2 BA.3 BA.2.3.20 BA.4/5 BA.4.6 BF.7 BQ.1 BQ1.1 XBB.1 XBB.1.5 XBB.1.16 EG.5 BA.2.86
Class 1
Class 2
Class 3
Undef.

Figure 3

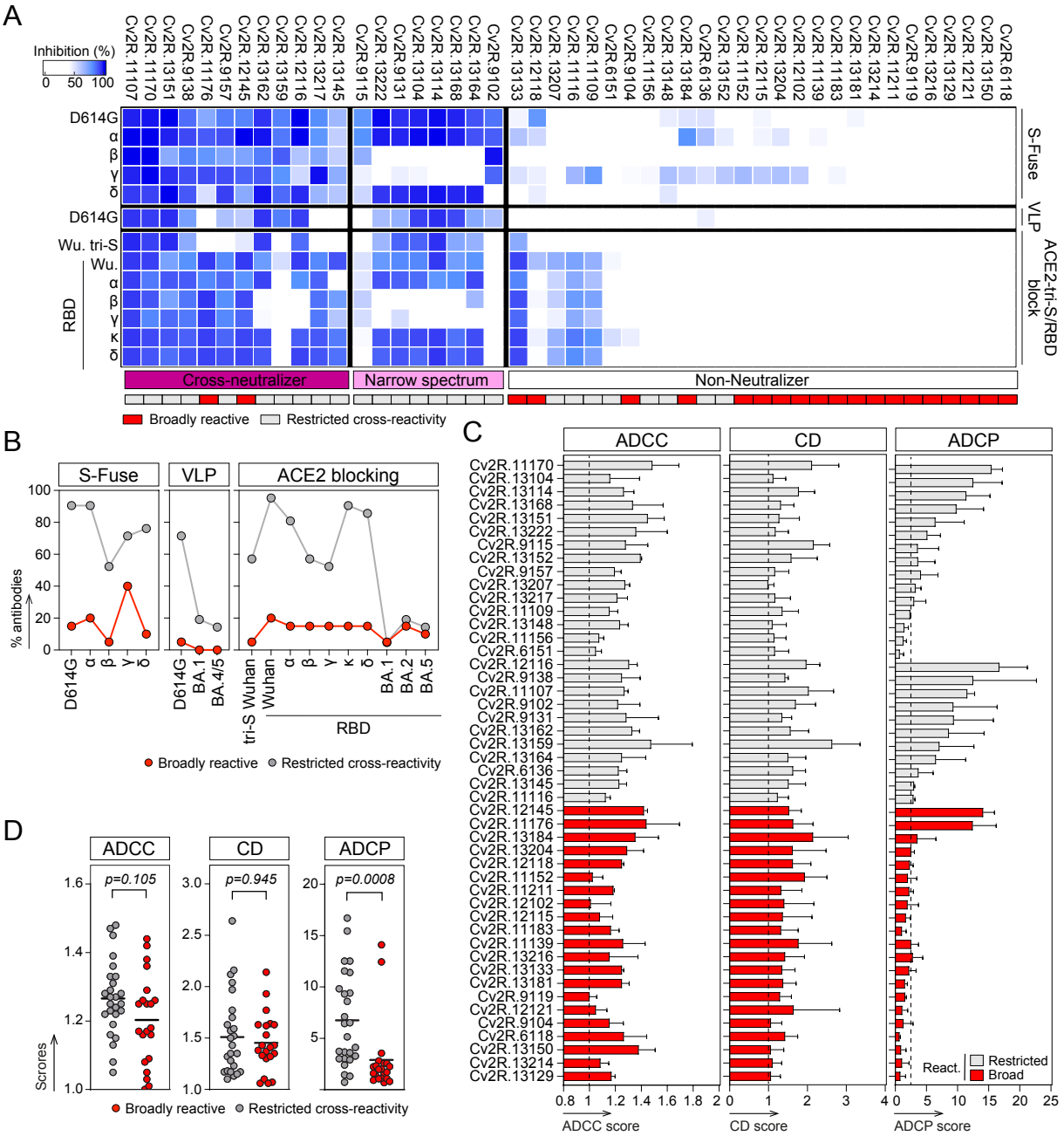
A
Inhibition (%)
0 50 100
Cv2R.11107 Cv2R.11170 Cv2R.13151 Cv2R.9138 Cv2R.11176 Cv2R.9157 Cv2R.12145 Cv2R.13162 Cv2R.13159 Cv2R.12116 Cv2R.13217 Cv2R.13145 Cv2R.9115 Cv2R.13222 Cv2R.9131 Cv2R.13104 Cv2R.13114 Cv2R.13168 Cv2R.13164 Cv2R.9102 Cv2R.13133 Cv2R.12118 Cv2R.13207 Cv2R.11116 Cv2R.11109 Cv2R.6151 Cv2R.9104 Cv2R.11156 Cv2R.13148 Cv2R.13184 Cv2R.6136 Cv2R.13152 Cv2R.11152 Cv2R.12115 Cv2R.13204 Cv2R.12102 Cv2R.11139 Cv2R.11183 Cv2R.13181 Cv2R.13214 Cv2R.11211 Cv2R.9119 Cv2R.13216 Cv2R.13129 Cv2R.12121 Cv2R.13150 Cv2R.6118
D614G
α
β
γ
δ
S-Fuse
D614G
VLP
Wu. tri-S
Wu.
RBD
α
β
γ
κ
δ
ACE2-tri-S/RBD block
Cross-neutralizer
Narrow spectrum
Non-Neutralizer
Broadly reactive
Restricted cross-reactivity
B
S-Fuse
VLP
ACE2 blocking
% antibodies
100
80
60
40
20
0
D614G α β γ δ
D614G BA.1 BA.4/5
tri-S Wuhan Wuhan α β γ κ δ BA.1 BA.2 BA.5
RBD
Broadly reactive
Restricted cross-reactivity
C
ADCC
CD
ADCP
Cv2R.11170 Cv2R.13104 Cv2R.13114 Cv2R.13168 Cv2R.13151 Cv2R.13222 Cv2R.9115 Cv2R.13152 Cv2R.9157 Cv2R.13207 Cv2R.13217 Cv2R.11109 Cv2R.13148 Cv2R.11156 Cv2R.6151 Cv2R.12116 Cv2R.9138 Cv2R.11107 Cv2R.9102 Cv2R.9131 Cv2R.13162 Cv2R.13159 Cv2R.13164 Cv2R.6136 Cv2R.13145 Cv2R.11116 Cv2R.12145 Cv2R.11176 Cv2R.13184 Cv2R.13204 Cv2R.12118 Cv2R.11152 Cv2R.11211 Cv2R.12102 Cv2R.12115 Cv2R.11183 Cv2R.11139 Cv2R.13216 Cv2R.13133 Cv2R.13181 Cv2R.9119 Cv2R.12121 Cv2R.9104 Cv2R.6118 Cv2R.13150 Cv2R.13214 Cv2R.13129
0.8 1 1.2 1.4 1.6 1.8 2
ADCC score
0 1 2 3 4
CD score
0 5 10 15 20 25
ADCP score
React.
Restricted
Broad
D
ADCC
CD
ADCP
p=0.105
p=0.945
p=0.0008
Scrores
1.0 1.2 1.4 1.6
1.0 1.5 2.0 2.5 3.0
5 10 15 20
Broadly reactive
Restricted cross-reactivity

Figure 4

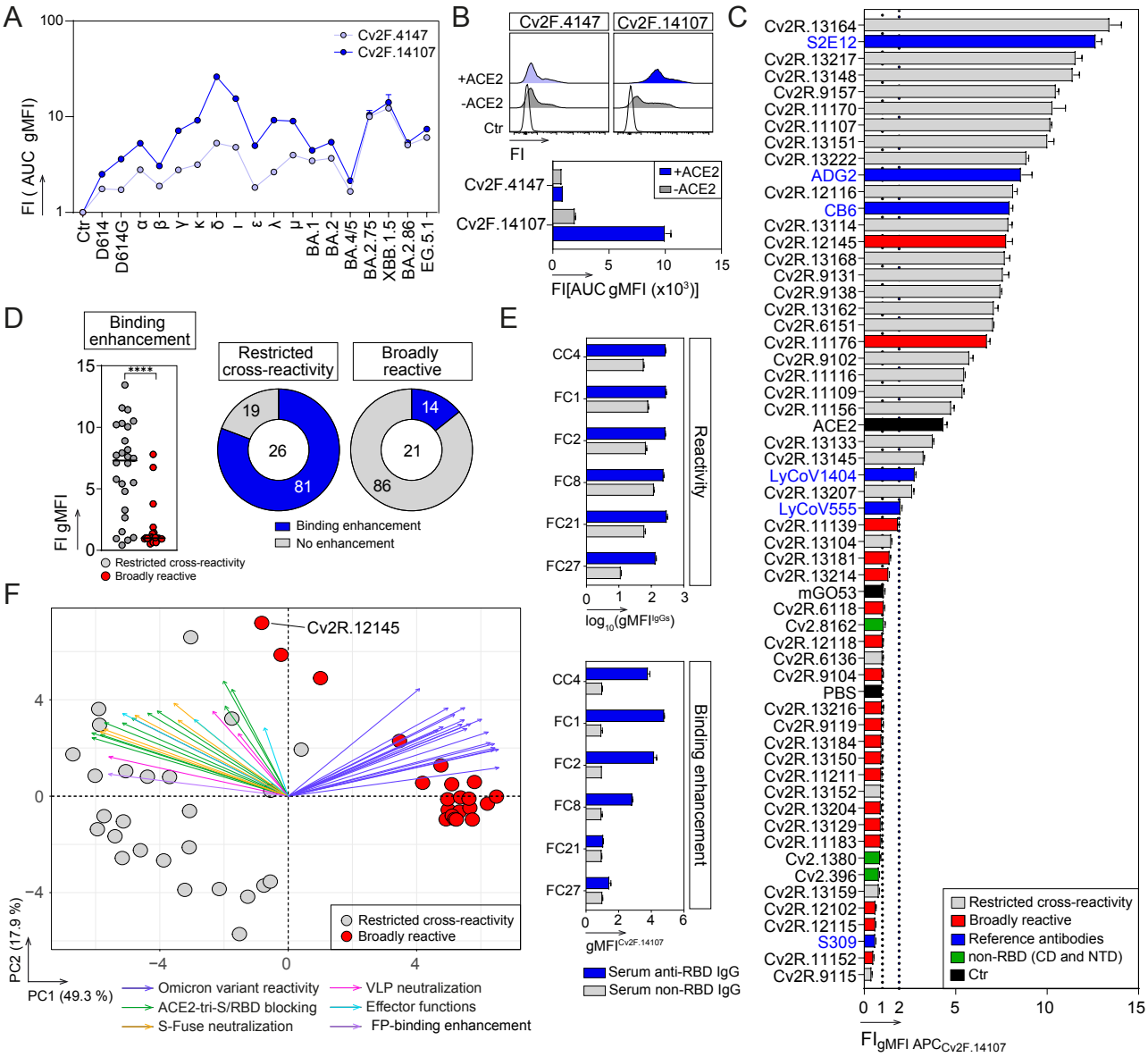
A
Cv2F.4147
Cv2F.14107
FI (AUC gMFI)
Ctr
D614
D614G
α
β
γ
κ
δ
ι
ε
λ
μ
BA.1
BA.2
BA.4/5
BA.2.75
XBB.1.5
BA.2.86
EG.5.1
B
Cv2F.4147
Cv2F.14107
+ACE2
-ACE2
Ctr
FI
FI[AUC gMFI (x10³)]
C
Cv2R.13164
S2E12
Cv2R.13217
Cv2R.13148
Cv2R.9157
Cv2R.11170
Cv2R.11107
Cv2R.13151
Cv2R.13222
ADG2
Cv2R.12116
CB6
Cv2R.13114
Cv2R.12145
Cv2R.13168
Cv2R.9131
Cv2R.9138
Cv2R.13162
Cv2R.6151
Cv2R.11176
Cv2R.9102
Cv2R.11116
Cv2R.11109
Cv2R.11156
ACE2
Cv2R.13133
Cv2R.13145
LyCoV1404
Cv2R.13207
LyCoV555
Cv2R.11139
Cv2R.13104
Cv2R.13181
Cv2R.13214
mGO53
Cv2R.6118
Cv2.8162
Cv2R.12118
Cv2R.6136
Cv2R.9104
PBS
Cv2R.13216
Cv2R.9119
Cv2R.13184
Cv2R.13150
Cv2R.11211
Cv2R.13152
Cv2R.13204
Cv2R.13129
Cv2R.11183
Cv2.1380
Cv2.396
Cv2R.13159
Cv2R.12102
Cv2R.12115
S309
Cv2R.11152
Cv2R.9115
Restricted cross-reactivity
Broadly reactive
Reference antibodies
non-RBD (CD and NTD)
Ctr
FI gMFI APC Cv2F.14107
D
Binding enhancement
****
FI gMFI
Restricted cross-reactivity
Broadly reactive
Restricted cross-reactivity
Broadly reactive
19
26
81
14
21
86
Binding enhancement
No enhancement
E
CC4
FC1
FC2
FC8
FC21
FC27
Reactivity
log10(gMFI IgGs)
Binding enhancement
gMFI Cv2F.14107
Serum anti-RBD IgG
Serum non-RBD IgG
F
Cv2R.12145
PC2 (17.9 %)
PC1 (49.3 %)
Restricted cross-reactivity
Broadly reactive
Omicron variant reactivity
ACE2-tri-S/RBD blocking
S-Fuse neutralization
VLP neutralization
Effector functions
FP-binding enhancement

Figure 5

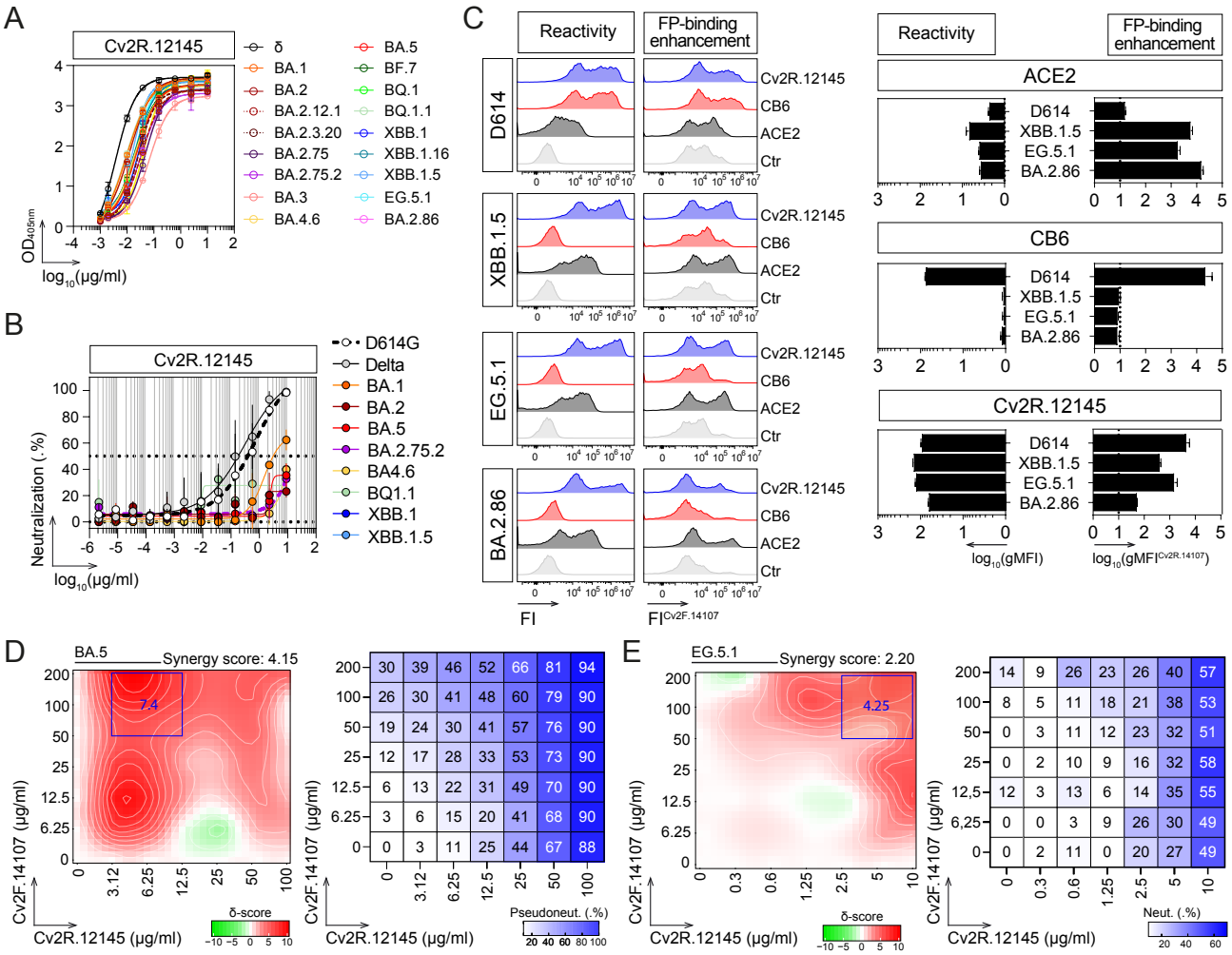
A
Cv2R.12145
δ
BA.1
BA.2
BA.2.12.1
BA.2.3.20
BA.2.75
BA.2.75.2
BA.3
BA.4.6
BA.5
BF.7
BQ.1
BQ.1.1
XBB.1
XBB.1.16
XBB.1.5
EG.5.1
BA.2.86
OD405nm
log10(µg/ml)
B
Cv2R.12145
D614G
Delta
BA.1
BA.2
BA.5
BA.2.75.2
BA4.6
BQ1.1
XBB.1
XBB.1.5
Neutralization (.%)
log10(µg/ml)
C
Reactivity
FP-binding enhancement
D614
XBB.1.5
EG.5.1
BA.2.86
Cv2R.12145
CB6
ACE2
Ctr
FI
FICv2F.14107
ACE2
CB6
Cv2R.12145
D614
XBB.1.5
EG.5.1
BA.2.86
log10(gMFI)
log10(gMFICv2R.14107)
D
BA.5
Synergy score: 4.15
7.4
Cv2F.14107 (µg/ml)
Cv2R.12145 (µg/ml)
δ-score
Pseudoneut. (.%)
E
EG.5.1
Synergy score: 2.20
4.25
Neut. (.%)

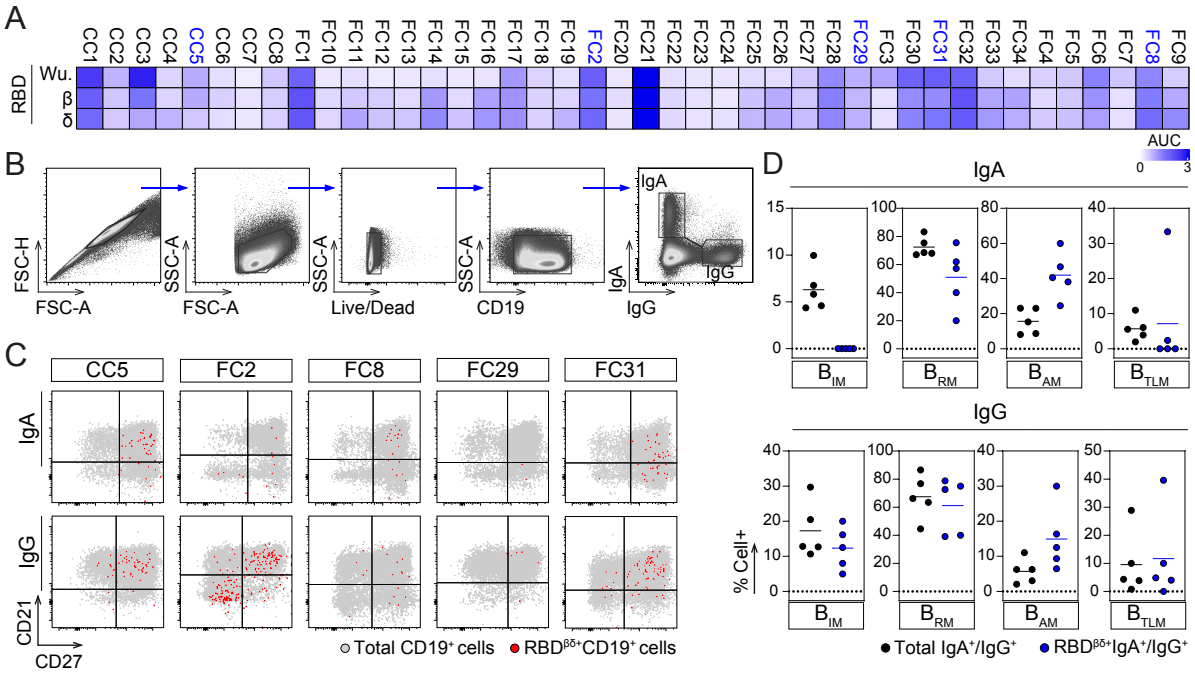

Figure S1. RBD-seroreactivity and -memory B-cell sorting. (**A**) Heatmap comparing the ELISA IgG seroreactivity of COVID-19 convalescents against purified recombinant Wuhan (Wu.), Beta (β), and Delta (δ) RBD proteins. Cells are color-coded according to the area under curve (AUC) values obtained by ELISA titrations. Blue-labeled donor codes indicate the samples selected for the flow cytometry B-cell sorting. (**B**) Flow cytometry plots presenting the gating strategy used to identify and single-cell sort SARS-CoV-2 RBDβδ^{+}-binding memory B cells. SSC, side scatter; FSC, forward scatter. (**C**) Flow cytometric plots showing for each donor the overlays of CD21 and CD27 stainings on total CD19^{+} cells (gray) with SARS-CoV-2 RBDβδ^{+} cells (red). (**D**) Scatter plots comparing the distribution of B-cell subsets between total (black) and SARS-CoV-2 RBDβδ^{+} (blue) IgG^{+} and IgA^{+} memory B cells (n = 5 donors): B_{IM} (intermediate memory, CD27^{-}CD21^{+}), B_{RM} (resting memory, CD27^{+}CD21^{+}), B_{AM} (activated memory, CD27^{+}CD21^{-}), and B_{TLM} (tissue-like memory, CD27^{-}CD21^{-}).

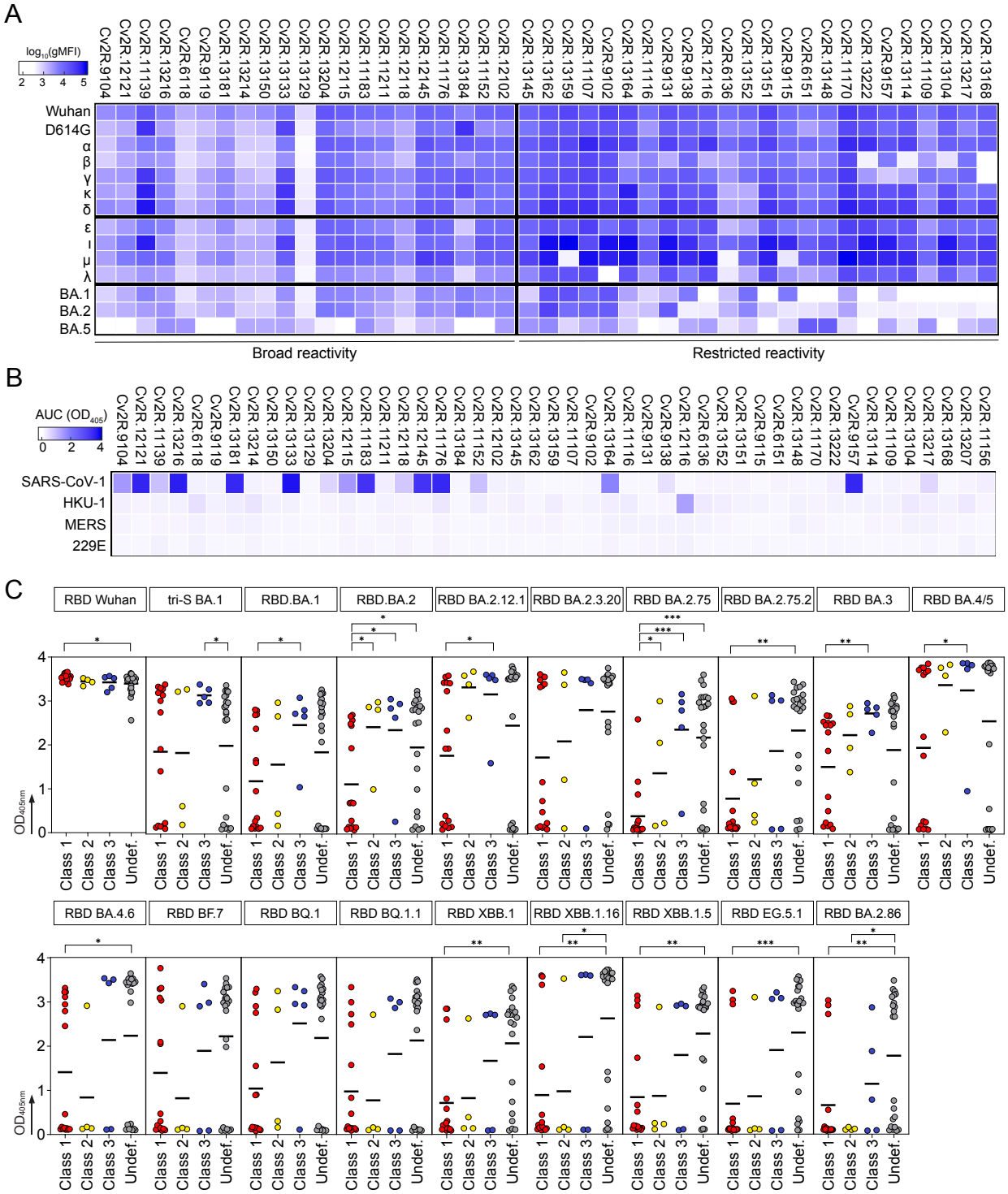

Figure S2. Reactivity profiling of human anti-RBD antibodies. (**A**) Heatmap comparing the reactivity profiles of anti-RBD across on 293F-cell transfectants expressing spike proteins from various SARS-CoV-2 variants. Cells are color-coded according to $\log_{10}$ geometric mean fluorescence intensity (gMFI) values, with dark blue colors indicating strong reactivities. Antibodies were categorized as either broadly reactive (red) or with a more restricted cross-reactivity (grey). (**B**) Heatmap comparing the ELISA reactivity of anti-RBD antibodies - measured as AUC from antibody titrations - against purified recombinant SARS-CoV-1, HKU-1, MERS-CoV, 229E tri-S proteins. Dark blue cells indicate high reactivities. Data correspond to mean of duplicate values. (**C**) Scatter plots comparing the anti-RBD antibody reactivities against RBD proteins from Wuhan and Omicron variants determined by ELISA. Antibody groups were defined based on RBD classes [1, 2, 3 and undefined (undef.)] and compared using Mann-Whitney's test. ***, $p < 0.001$; **, $p < 0.01$; *, $p < 0.05$.

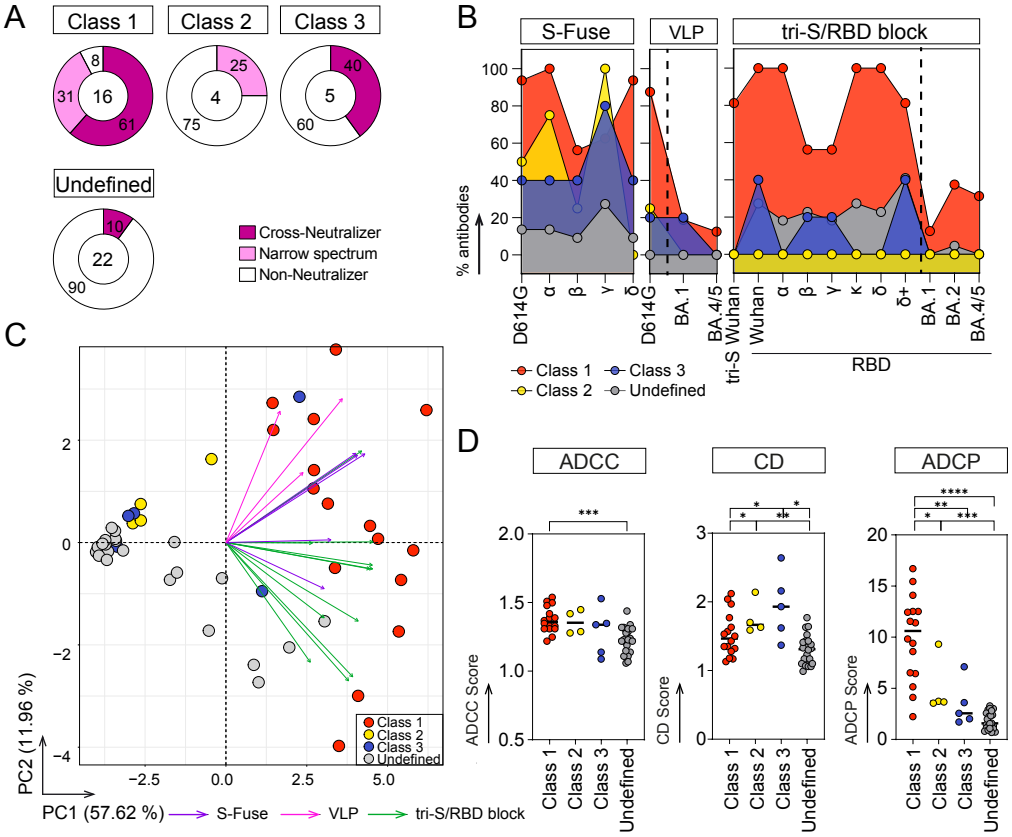

Figure S3. Functional profiling of anti-RBD antibody classes. (**A**) Donut charts comparing the distribution of cross-neutralizing (purple), narrow spectrum (pink), or non-neutralizing (white) antibodies according to their RBD class (1, 2, 3 and undefined). (**B**) Graph comparing the neutralization profiles of anti-RBD antibodies as determined in the S-fuse and VLP neutralization assays, and ACE2-tri-S or -RBD blocking ELISA assay according to their RBD class as defined in Fig.2B. (**C**) PCA 2D-plot showing the neutralization variables (arrows; S-fuse, VLP, ACE2-tri-S or -RBD blocking assays) discriminating human anti-RBD antibodies (n = 47). Dots represent single antibodies, color-coded based on their RBD class. (**D**) Scatter plots comparing the ADCC, CD, and ADCP activities of anti-RBD specific antibodies according to their RBD class. Groups were compared using Mann-Whitney's test. ****, $p < 0.0001$; ***, $p < 0.001$; **, $p < 0.01$; *, $p < 0.05$.

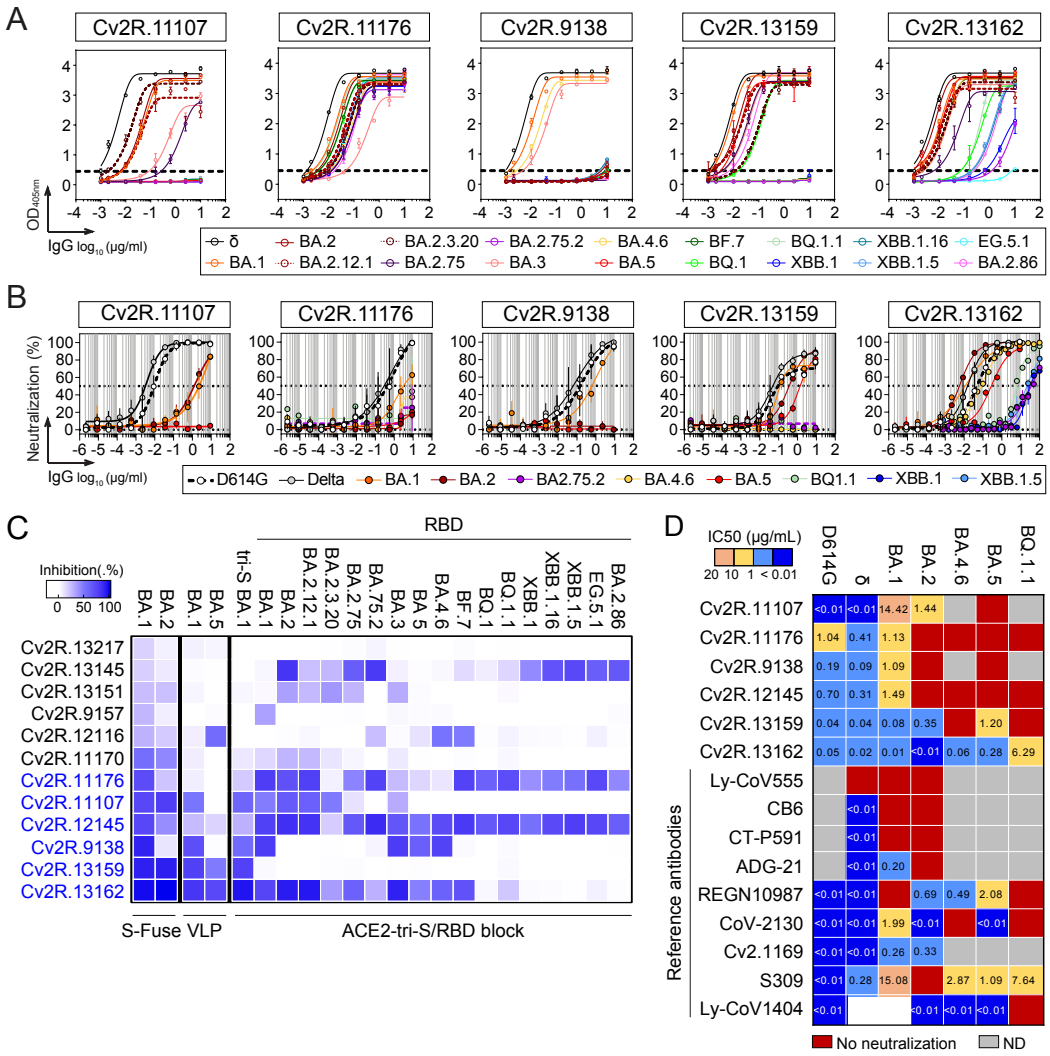

Figure S4. SARS-CoV-2 cross-reactivity and -neutralization profiles of anti-RBD neutralizers. (**A**) ELISA graph comparing the binding curves of the five selected potent anti-RBD IgG antibodies against SARS-CoV-2 RBD proteins from Delta and Omicron variants Error bars represent the SD of duplicate values. (**B**) Same as in (A) but for in vitro neutralization in the S-Fuse assays using authentic viruses. (**C**) Heatmap comparing the neutralizing activities of potent anti-RBD antibodies as determined in the S-fuse and VLP neutralization assays, and ACE2-tri-S or -RBD blocking ELISA assay. Mean of duplicate values are shown. Dark blue colors indicate strongest inhibition percentages, while white corresponds to no inhibition. Blue-labeled antibodies (>70% SARS-CoV-2 BA.1 neutralization) were considered as the most potent. (**D**) Table comparing the IC_{50} values of the 6 most potent cross-neutralizing anti-RBD antibodies and reference antibodies against SARS-CoV-2 D614G, Delta, and Omicron variants measured in the S-Fuse neutralization assay as shown in (A). ND, not determined.

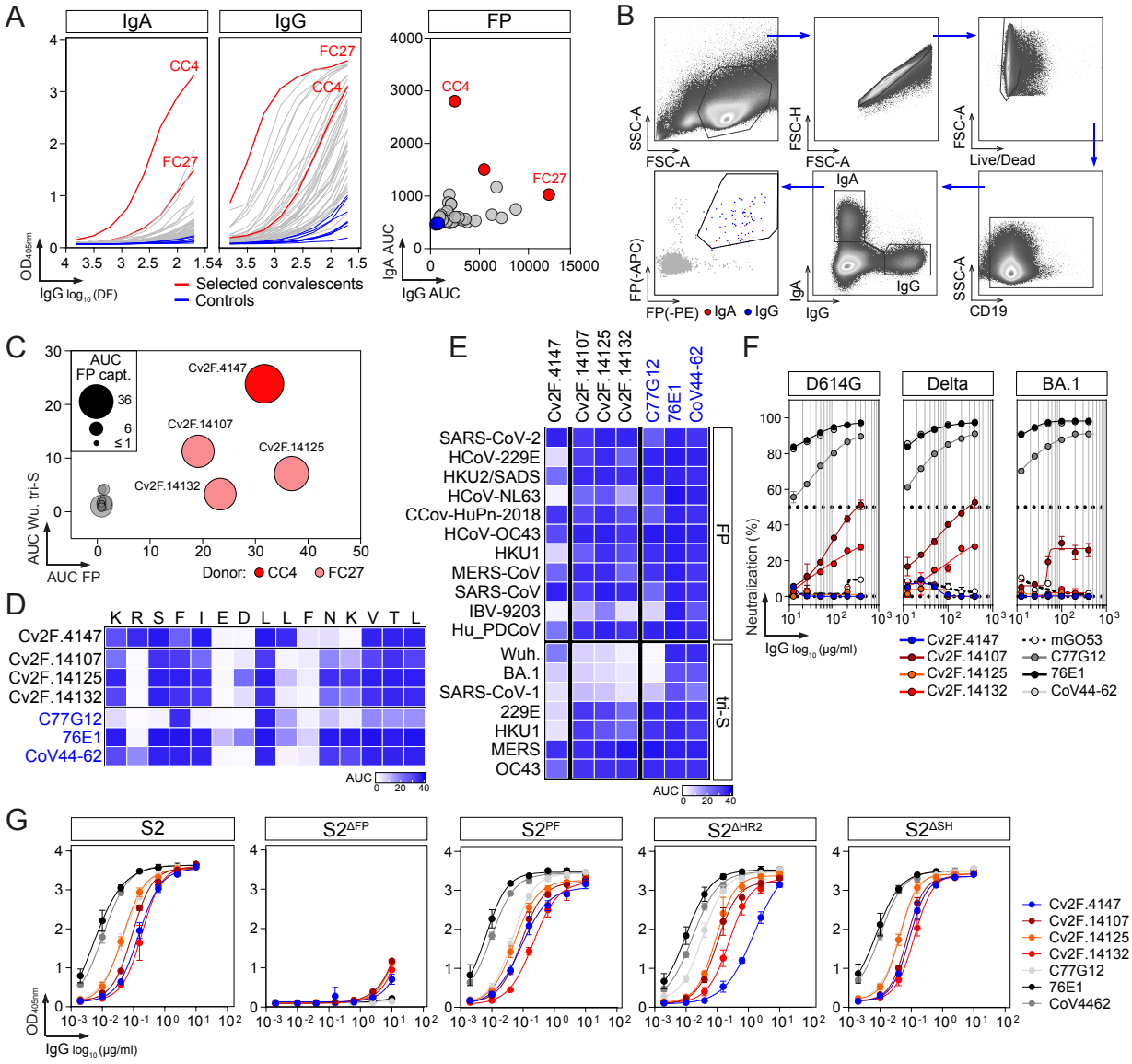

Figure S5. Human SARS-CoV-2 FP-specific memory B-cell antibody cloning and characterization. (**A**) ELISA graphs (left) comparing the IgG and IgA seroreactivities from COVID-19 convalescent individuals (n=42, non-blue lines) against SARS-CoV-2 fusion peptide (FP). Mean of duplicate values are shown. Red and blue lines correspond to the convalescent donors selected for single B-cell sorting (CC4 and FC27) and healthy individual controls (n=8), respectively. DF, dilution factors. Dot plot (right) comparing IgG and IgA FP-seroreactivity, shown as AUC values derived from the ELISA titrations. (**B**) Flow cytometry plots presenting the gating strategy used to identify and single-cell FP-binding memory B cells from the PBMC of CC4 and FC27 donors. (**C**) Bubble plot comparing the ELISA binding of 17 human antibodies cloned from SARS-CoV-2 FP-captured IgG$^+$ and IgA$^+$ memory B cells of CC4 (blue) and FC27 (red) donors. The y-axis shows binding to Wuhan tri-S protein; the x-axis and bubble size represent binding to FP peptide measured by classical indirect and capture ELISA (capt.), respectively. Grey bubbles indicate non-reactive antibodies from both donors. Values correspond to mean AUC values calculated from duplicate titrations. (**D**) Heatmap comparing the ELISA binding of anti-FP peptides and reference antibodies to alanine-mutated FP peptides (mutated residues at the top). Values correspond to mean AUC values calculated from duplicate titrations, with dark blue cells indicating strong binding. (**E**) Same as in (D) but for fusion peptides and tri-S proteins from different coronaviruses. (**F**) Graphs comparing the SARS-CoV-2 neutralizing activity of anti-FP and reference antibodies as measured in the S-Fuse neutralization assay. Error bars represent the SD of duplicate values. (**G**) ELISA graphs comparing the binding of anti-FP and reference antibodies to pre- and post-fusion trimeric SARS-CoV-2 S2 subunits (S2 and S2^{PF}), and S2 protein versions deleted from the fusion peptide (S2$^{\Delta FP}$), heptad-repeat 2 (S2$^{\Delta HR2}$) or stem-helix (S2$^{\Delta SH}$). Error bars correspond the SD of duplicate values.

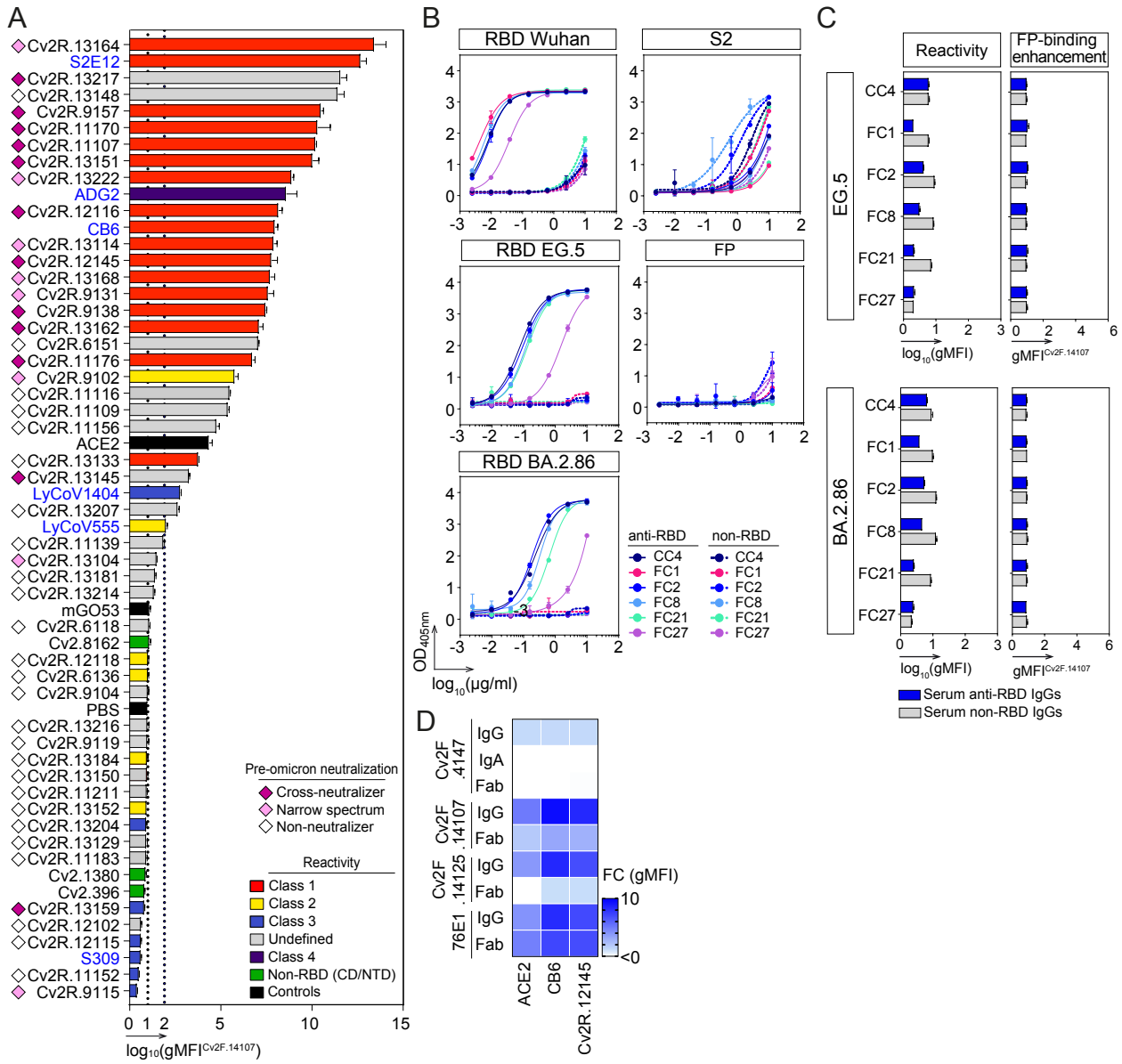

Figure S6. ACE2-mimetic activity of anti-RBD antibodies. (**A**) Bar graph comparing the enhanced binding of anti-FP Cv2F.14107 to Delta tri-S-expressing 293F cell transfectants in the presence of anti-RBD antibodies. Bars are color-coded according to the RBD class and show the means ± SD of duplicate values. Dotted lines indicate the basal gMFI (black) and a two-fold increase (blue). Diamond symbols on the left are color-coded according to the neutralization profiles on pre-Omicron viruses (see Fig.3A): cross-neutralizing (purple), narrow spectrum (pink), or non-neutralizing (white). (**B**) ELISA graphs comparing the binding of total anti-RBD and non-anti-RBD IgG antibodies purified from six convalescent sera against Wuhan, EG.5 and BA.2.86 RBD proteins, Wuhan S2 subunit and FP peptide. Error bars correspond to the SD of duplicate values. (**C**) Bar graphs comparing the EG.5 and BA2.86 Spike binding (left) and ACE2-mimetic capacity (right; enhanced Cv2F.14107 binding) measured by flow cytometry of total anti-RBD (blue) and non-RBD (grey) IgG antibodies purified from convalescent sera. Error bars represent the SD of duplicate values. (**D**) Heatmap comparing the ACE2-mimetic capacity of soluble ACE2, CB6, and Cv2R.12145 measured by flow cytometry on Delta spike-expressing 293F transfectants as enhanced binding of anti-FP antibodies (Cv2F.4147, Cv2F.14107, CV2F.14125 and 76E1) produced as recombinant IgG, IgA or Fab. Cells are color-coded based on the mean fold change (FC) of duplicate gMFI values relative to the no antibody control (means of duplicate values). Darker blue indicates a higher fold change signal intensity

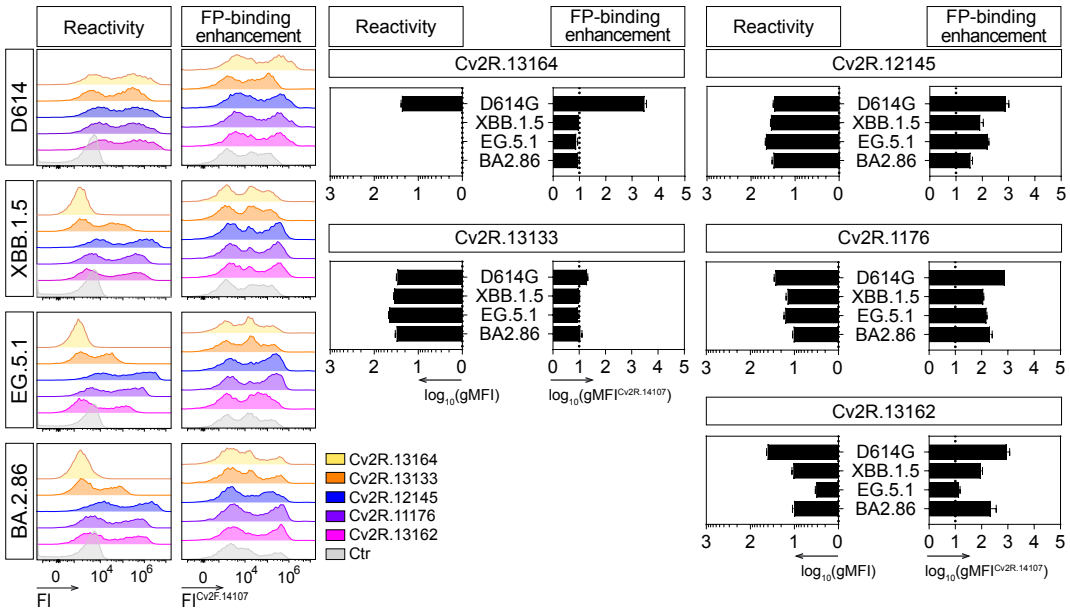

Figure S7. ACE2-mimetic activity of broadly reactive anti-RBD antibodies. Representative flow cytometry histograms (left) and bar graph (right) comparing the spike binding and ACE2-mimetic capacity (based on enhanced Cv2F.14107 binding) of 5 broadly reactive anti-RBD IgG antibodies as determined by flow cytometry using 4 different SARS-CoV-2 strains. Error bars in graphs represent the SD of duplicate values. Ctr, no antibody control.

Table S1. Immunoglobulin gene repertoire of human SARS-CoV-2 RBD memory B-cell antibodies.

			IgH									IgL							
							CDR_H3								CDR_L3				
mAb	Donor	B-cell subset	V_H	D_H	J_H	Subtype	Sequence (aa)	Length	(+)	(-)	V_H mut.	IgL	V_L	J_L	Sequence (AA)	Length	(+)	(-)	V_L mut.
Cv2R.11107	CC5	AM	1-58	2-2	6	α2	PHCNRTTCLDGMDV	14	2	2	4	κ	3-20	1	QQYDSSPWT	9	0	1	7
Cv2R.11109	CC5	RM	3-33	3-22	1	γ1	EARMYYLDNSGYQETPYFQH	20	2	3	12	κ	3-15	1	QQYNNWPPWT	10	0	0	3
Cv2R.11116	CC5	RM	1-3	1-1/3-16/-16	6	γ1	GAYNFWMDV	9	0	1	9	λ	6-57	3	QSYDSSNRV	9	1	1	1
Cv2R.11136	CC5	AM	1-2	3-3	6	α1	DLRFFYYGMDV	11	1	2	13	λ	2-8	2/3	SSYAGSNNLV	10	0	0	7
Cv2R.11137	CC5	RM	4-38	3-16	4	γ1	AAPTLITLGGVIAGEHDY	18	1	2	11	κ	1-5	4	QQYNGYSQT	9	0	0	5
Cv2R.11139	CC5	RM	3-11	2-15	4	γ1	SPKSRCNGGSCYPYYFDY	18	2	1	10	κ	3-20	4	QQYGSSPRLT	10	1	1	3
Cv2R.11152	CC5	RM	3-30	5-18/-5	4	γ1	DPIRYSYGQTGYLDY	15	1	2	3	λ	3-21	1	QVWDSTSDHFYV	12	1	2	3
Cv2R.11156	CC5	RM	3-48	2-15	4	γ1	AAAGVVAGFDY	11	0	1	4	λ	6-57	2/3	QSYDSSNQV	9	0	1	4
Cv2R.11160	CC5	RM	1-2	3-22	4	α1	MPQYYYDSSGYSDY	14	0	2	3	λ	2-14	1	SSYTSSSLYV	10	0	0	2
Cv2R.11170	CC5	RM	1-58	2-2	3	γ1	PYCNRTSCEDAFDI	14	1	3	4	κ	3-20	1	QQYGRSPWT	9	1	0	6
Cv2R.11176	CC5	RM	1-69	3-22	4	γ1	TTYYYDRSGYIRQGDYFDY	19	2	3	9	λ	1-40	3	QSYDSSLSGCV	11	0	1	5
Cv2R.11178	CC5	RM	3-53	7-27	4	α1	ALYLTLDS	8	0	1	8	κ	1-33/1D-33	4	QQYDNLPQLT	10	0	1	4
Cv2R.11183	CC5	RM	1-69/1-69D	1-26	4	γ1	GDSGSYYGGGFDY	13	0	2	6	λ	1-51	2/3	GTWDSSLSAL	10	0	1	4
Cv2R.11211	CC5	AM	3-9	3-10	5	γ1	GLYGSGSPWVNWFDP	15	0	1	3	κ	1-12/1D-12	3	QQANSFPLT	9	0	0	5
Cv2R.6111	FC2	RM	3-66	3-16/-16/5-24	4	γ1	DVLEGAFDY	9	0	3	6	κ	1-9	4	QQLNSYPQLT	10	0	0	2
Cv2R.6118	FC2	RM	4-39	2-2	6	γ3	GVVPATYHYYYYIDV	15	1	1	12	κ	3-20	5	QQYGSF	6	0	0	7
Cv2R.6136	FC2	RM	1-2	3-10/-16	2	γ3	DHGGRFWDWYFDL	13	2	3	3	λ	2-8	3	SSYAGSNNP	9	0	0	1
Cv2R.6151	FC2	AM	4-59	5-12	4	γ1	LEWLRGAFDY	10	1	2	5	λ	6-57	2/3	QSYDSGIVV	9	0	1	4
Cv2R.9102	FC8	AM	1-46	3-22	5	γ1	DPPLGAYYYDSLPFDP	16	0	3	3	λ	6-57	3	QSYDSSNHNWV	11	1	1	4
Cv2R.9104	FC8	AM	3-23	6-19	2	γ1	EAVAGTDWYFDL	12	0	3	5	κ	1-39/1D-39	4	QQSYSTPPIT	10	0	0	3
Cv2R.9107	FC8	TLM	1-18	3-16	4	γ1	VRDDYVWGSYYYFDY	15	1	3	1	κ	3-15	3	QQYNNWPPIFT	11	0	0	3
Cv2R.9115	FC8	AM	3-9	2-2	4	γ3	DSEDCSSVTCFLDY	14	0	4	2	κ	4-1	1	QQYYSTPQT	9	0	0	5
Cv2R.9119	FC8	AM	1-46	5-18/-5	6	γ1	DRGWIPHTAGMDV	13	2	2	4	κ	1-5	1	QQYNSYSWT	9	0	0	6
Cv2R.9131	FC8	RM	3-53	3-10	4	γ1	DSGFGELD	8	0	3	3	κ	1-33/1D-33	5	QQYDNLPRT	9	1	1	2
Cv2R.9138	FC8	RM	3-33	3-22	6	γ1	VLMGYDSRGYIGHYYGMDV	19	2	2	5	κ	1-33/1D-33	2/3	QQYDNLPPVT	10	0	1	3
Cv2R.9157	FC8	AM	3-9	5-12	4	γ1	YDPLHRSYLDY	11	2	2	6	κ	1-33/1D-33	3	QQYDNLLGT	9	0	1	7
Cv2R.12102	FC29	RM	4-39	4-23	4	γ1	DYGGNSNYFHY	11	1	1	4	κ	1-13/1D-13	4	QQFNSYPLT	9	0	0	10
Cv2R.12115	FC29	RM	4-31	4-23	4	γ1	DYGGNSNYFDY	11	0	2	5	κ	1-13/1D-13	4	QQFNSYPLT	9	0	0	6
Cv2R.12116	FC29	AM	3-66	5-12	6	γ1	PHLRSGMDV	9	2	1	8	κ	1-33/1D-33	3	QQYDNLPVT	9	0	1	11
Cv2R.12118	FC29	RM	3-13	6-13/7-27	4	γ1	GFSWGSFHYYFEH	13	2	1	12	κ	1-39/1D-39	1	QQSYSSPPWT	10	0	0	8
Cv2R.12121	FC29	RM	3-23	3-22	4	γ1	VHLAYYYDSSDDGHY	15	2	3	7	κ	2-30	4	MQGTHWPPT	9	1	0	2
Cv2R.12124	FC29	RM	3-30	3-10	6	γ1	CLWRVRGGRPGLHYYYAMDV	20	4	1	8	λ	2-14	3	SSYTSSSTVV	10	0	0	7
Cv2R.12145	FC29	RM	3-74	3-22	4	γ1	VPRGYYDRSGYYTALHYFDY	20	3	2	6	κ	4-1	2	QQYYSTPYT	9	0	0	8
Cv2R.12153	FC29	RM	3-66	/	4	γ1	GLDLYFDY	8	0	2	1	κ	1-9	4	QQLNSYPPA	9	0	0	4
Cv2R.13104	FC31	AM	3-66	3-22	1	α1	DGYYDSSGYFSEYFQH	16	1	3	4	κ	3-11	4	QQRSNSPLT	9	1	0	1
Cv2R.13114	FC31	AM	3-53	3-16	4	α1	DWGELYFDY	9	0	3	5	κ	3-20	4	QQYGSSRRT	9	2	0	4
Cv2R.13129	FC31	RM	4-39	4-17	4	γ1	LQFYRDYSFDY	11	1	2	5	λ	2-14	2/3	SSYTSSSTYVV	11	0	0	3
Cv2R.13133	FC31	RM	3-30	2-15	6	γ1	DFVGGFCNGGSCYPYYGMDV	20	0	2	7	λ	6-57	2/3	QSYDSSNHVV	10	1	1	1
Cv2R.13145	FC31	RM	4-59	5-12	4	γ3	RLWLRGTFDY	10	2	1	7	λ	6-57	2/3	QSYDSSNQYLV	11	0	1	2
Cv2R.13148	FC31	RM	3-48	3-3/3-3	3	γ1	LGWLRGAFDI	10	1	1	3	λ	6-57	3	QSYDSTNWV	9	0	1	4
Cv2R.13150	FC31	RM	3-11	3-3	4	γ1	FSPYYDVYSGYFDY	14	0	2	3	λ	2-23	2/3	CSYAGNTVI	9	0	0	3
Cv2R.13151	FC31	RM	4-39	6-13/-19/-25	4	γ1	RMGMFDF	7	1	1	10	κ	1-NL1	1	QQYYSPPPET	10	0	1	9
Cv2R.13152	FC31	AM	1-69	6-13/-25	6	α1	DRGSSSQGSNYYMDV	15	1	2	5	λ	1-40	1	QSYDSSLIDSV	11	0	2	8
Cv2R.13159	FC31	RM	3-30	2-2	4	γ1	DSEDCSSFTCYLDY	14	0	4	4	κ	4-1	3	QQYYSTPFT	9	0	0	5
Cv2R.13162	FC31	AM	3-53	1-26	6	γ1	DLLQAGGMDV	10	0	2	4	κ	1-33/1D-33	3	QQYDNVPPA	9	0	1	4
Cv2R.13164	FC31	RM	3-43	3-10	6	α1	DMTVEVGSGNYYIGYYYGMDV	21	0	3	7	κ	1-5	1	QQYNSYSRT	9	1	0	3
Cv2R.13168	FC31	AM	3-53	4-17	4	γ1	DYGDFYFDY	9	0	3	4	κ	3-15	1	QQYYNWPRT	9	1	0	6
Cv2R.13181	FC31	RM	1-46	2-2	4	γ1	DASIIPSTSCADY	13	0	2	7	κ	3-11	1	QQRSNWLWT	9	1	0	5
Cv2R.13184	FC31	RM	1-69	3-10	4	α1	EGAYSGSGAQYYFDY	15	0	2	3	λ	1-40	1	QSYDSSLNGCV	11	0	1	8
Cv2R.13203	FC31	RM	3-53	/	4	α1	DLGWHYFDY	9	1	2	2	κ	1-9	5	QQLNSYPSPST	11	0	0	3
Cv2R.13204	FC31	RM	3-11	3-3	3	γ1	GLGWLLDELDAFDI	14	0	4	4	κ	3-20	5	QQYYSSFT	8	0	0	6
Cv2R.13207	FC31	RM	4-39	3-22	3	γ1	GTNYFDSSGSYRREAFDI	18	2	3	10	κ	1-5	2	QQYNSYLYT	9	0	0	10
Cv2R.13214	FC31	RM	1-46	2-2	3	α1	DIVLVPAADAFDI	13	0	3	2	κ	3-11	3	QQRSNWPLIFT	11	1	0	4
Cv2R.13216	FC31	RM	3-48	1-26/2-15/-21	6	γ1	HKGGLSYYYYGMDV	14	2	1	4	κ	1-39/1D-39	1	QQSYSTPGT	9	0	0	2
Cv2R.13217	FC31	RM	3-9	3-16	3	γ1	GRLGELLDAFDI	12	1	3	6	κ	3-15	1	QQYNNWPLWT	10	0	0	3
Cv2R.13222	FC31	AM	4-38	7-27	4	γ1	QLGMTDY	7	0	1	0	κ	1-NL1	2	QQYYSTPYT	9	0	0	7

(-) and (+) indicate the numbers of negatively and positively charged amminoacids in the IgH complementary determining region (CDR3), respectively. aa, amino acid; mut., number of somatic mutations.
RM, resting memory; AM activated memory; TLM, tissu-like memory.

Table S2. Binding profiles of human SARS-CoV-2 RBD memory B-cell antibodies.

| mAb | Reactivity profile | Epitope | ELISA reactivity (OD) | | |

Table S3. Antiviral functions of human SARS-CoV-2 RBD memory B-cell antibodies.

mAb	Neutralization profile	S-Fuse (% neut.)							VLP (% inh.)			ACE2-tri-S/RBD-block (% inh.)																															Effector assays			
												Basic panel										Extended Omicron panel																							
													RBD										RBD																						
		D614G	α	β	γ	δ	BA.1	BA.2	D614G	BA.1	BA.5	tri-S Wu.	Wu.	α	β	γ	κ	δ	BA.1	BA.2	BA.5	tri-SBA.1	BA.1	BA.2	BA.2.12.1	BA.2.75	BA.3	BA.5	BA4.6	BA2.75.2	BA2.3.20	BQ.1	BQ.1.1	BF.7	XBB.1	XBB.1.5	XBB.1.16	EG.5.1	BA.2.86	ADCC (Fold	ADCP (%)	CDC (Score)	ACE2-mim.
Cv2R.11107	Broad	98	100	100	98	95	75	80	95	50	0	97	95	94	95	94	95	94	7	58	13	59	47	65	62	10	30	0	0	0	48	0	0	0	0	0	0	0	0	1.3	11.6	2.0	10.2
Cv2R.11109	Non-/partial	34	26	12	77	21	13	0	19	9	9	1	68	63	74	61	79	73	33	15	0	ND	ND	ND	ND	ND	ND	ND	ND	ND	ND	ND	ND	ND	ND	ND	ND	ND	ND	1.2	2.4	1.4	5.4
Cv2R.11116	Non-/partial	34	18	18	66	19	13	7	17	6	4	0	74	71	77	71	84	81	27	20	5	ND	ND	ND	ND	ND	ND	ND	ND	ND	ND	ND	ND	ND	ND	ND	ND	ND	ND	1.1	2.9	1.2	5.5
Cv2R.11136	ND	ND	ND	ND	ND	ND	ND	ND	ND	ND	ND	ND	ND	ND	ND	ND	ND	ND	ND	ND	ND	ND	ND	ND	ND	ND	ND	ND	ND	ND	ND	ND	ND	ND	ND	ND	ND	ND	ND	ND	ND	ND	ND
Cv2R.11137	ND	ND	ND	ND	ND	ND	ND	ND	ND	ND	ND	ND	ND	ND	ND	ND	ND	ND	ND	ND	ND	ND	ND	ND	ND	ND	ND	ND	ND	ND	ND	ND	ND	ND	ND	ND	ND	ND	ND	ND	ND	ND	ND
Cv2R.11139	Non-/partial	19	43	23	34	15	ND	ND	0	0	0	0	0	0	0	0	0	0	0	0	0	ND	ND	ND	ND	ND	ND	ND	ND	ND	ND	ND	ND	ND	ND	ND	ND	ND	ND	1.3	2.6	1.8	1.9
Cv2R.11152	Non-/partial	15	17	14	65	5	ND	ND	23	0	0	0	0	0	0	0	0	0	0	0	0	ND	ND	ND	ND	ND	ND	ND	ND	ND	ND	ND	ND	ND	ND	ND	ND	ND	ND	1.0	2.0	1.9	0.5
Cv2R.11156	Non-/partial	22	1	0	43	0	ND	ND	16	10	9	0	0	7	4	0	24	0	7	2	0	ND	ND	ND	ND	ND	ND	ND	ND	ND	ND	ND	ND	ND	ND	ND	ND	ND	ND	1.1	1.3	1.1	4.8
Cv2R.11160	ND	ND	ND	ND	ND	ND	ND	ND	ND	ND	ND	ND	ND	ND	ND	ND	ND	ND	ND	ND	ND	ND	ND	ND	ND	ND	ND	ND	ND	ND	ND	ND	ND	ND	ND	ND	ND	ND	ND	ND	ND	ND	ND
Cv2R.11170	Broad	99	100	100	100	93	54	43	94	6	0	94	94	84	91	82	92	91	0	13	0	8	14	26	25	3	8	0	0	0	10	0	3	1	0	0	0	0	0	1.5	15.5	2.1	10.3
Cv2R.11176	Broad	71	90	78	92	51	73	21	19	6	0	37	95	82	96	94	94	94	48	58	15	19	80	70	78	45	24	14	9	77	5	61	72	78	40	53	48	75	43	1.4	12.4	1.6	6.7
Cv2R.11178	ND	ND	ND	ND	ND	ND	ND	ND	ND	ND	ND	ND	ND	ND	ND	ND	ND	ND	ND	ND	ND	ND	ND	ND	ND	ND	ND	ND	ND	ND	ND	ND	ND	ND	ND	ND	ND	ND	ND	ND	ND	ND	ND
Cv2R.11183	Non-/partial	1	11	23	43	2	ND	ND	21	0	0	0	0	0	0	0	0	0	0	0	0	ND	ND	ND	ND	ND	ND	ND	ND	ND	ND	ND	ND	ND	ND	ND	ND	ND	ND	1.2	1.1	1.3	0.9
Cv2R.11211	Non-/partial	16	9	9	31	0	ND	ND	22	0	0	0	0	0	0	0	0	0	0	0	0	ND	ND	ND	ND	ND	ND	ND	ND	ND	ND	ND	ND	ND	ND	ND	ND	ND	ND	1.2	2.3	1.3	1.0
Cv2R.6111	ND	ND	ND	ND	ND	ND	ND	ND	ND	ND	ND	ND	ND	ND	ND	ND	ND	ND	ND	ND	ND	ND	ND	ND	ND	ND	ND	ND	ND	ND	ND	ND	ND	ND	ND	ND	ND	ND	ND	ND	ND	ND	ND
Cv2R.6118	Non-/partial	7	23	0	13	0	ND	ND	0	0	0	0	0	0	0	0	0	0	0	0	0	ND	ND	ND	ND	ND	ND	ND	ND	ND	ND	ND	ND	ND	ND	ND	ND	ND	ND	1.3	0.7	1.4	1.1
Cv2R.6136	Non-/partial	50	63	34	51	0	21	29	45	0	1	0	0	0	0	0	0	0	0	0	0	ND	ND	ND	ND	ND	ND	ND	ND	ND	ND	ND	ND	ND	ND	ND	ND	ND	ND	1.2	3.7	1.6	1.0
Cv2R.6151	Non-/partial	22	17	6	33	11	ND	ND	21	0	2	0	42	16	28	0	52	38	0	0	17	ND	ND	ND	ND	ND	ND	ND	ND	ND	ND	ND	ND	ND	ND	ND	ND	ND	ND	1.0	0.7	1.2	7.1
Cv2R.9102	Narrow	86	89	99	88	13	83	92	63	36	8	8	0	0	0	0	10	0	0	0	24	9	0	0	0	0	0	0	0	1	0	0	0	0	ND	ND	ND	ND	ND	1.2	9.3	1.7	5.8
Cv2R.9104	Non-/partial	31	30	21	41	16	ND	ND	0	0	3	2	34	26	9	0	46	34	3	0	44	ND	ND	ND	ND	ND	ND	ND	ND	ND	ND	ND	ND	ND	ND	ND	ND	ND	ND	1.2	1.3	1.1	1.0
Cv2R.9107	ND	ND	ND	ND	ND	ND	ND	ND	ND	ND	ND	ND	ND	ND	ND	ND	ND	ND	ND	ND	ND	ND	ND	ND	ND	ND	ND	ND	ND	ND	ND	ND	ND	ND	ND	ND	ND	ND	ND	ND	ND	ND	ND
Cv2R.9115	Narrow	79	80	69	45	55	46	18	31	10	3	10	51	49	58	52	42	33	34	27	0	6	3	5	2	3	0	0	0	0	1	0	1	1	0	0	0	0	0	1.3	3.6	2.2	0.4
Cv2R.9119	Non-/partial	9	16	4	0	4	ND	ND	1	4	2	0	0	1	0	0	0	0	0	7	0	ND	ND	ND	ND	ND	ND	ND	ND	ND	ND	ND	ND	ND	ND	ND	ND	ND	ND	1.0	1.6	1.3	1.0
Cv2R.9131	Narrow	96	98	14	46	96	72	94	68	9	8	88	82	89	29	52	91	91	23	60	15	ND	ND	ND	ND	ND	ND	ND	ND	ND	ND	ND	ND	ND	ND	ND	ND	ND	ND	1.3	9.4	1.4	7.6
Cv2R.9138	Broad	87	93	83	92	90	92	9	74	72	1	70	80	90	85	84	89	91	71	0	70	56	80	0	0	0	80	63	77	4	1	0	2	2	0	0	0	0	0	1.3	12.5	1.4	7.5
Cv2R.9157	Broad	84	92	73	92	94	26	6	62	0	1	40	82	87	81	82	88	91	1	0	0	0	34	0	0	1	3	1	2	0	1	0	0	0	0	0	0	0	1	1.2	4.1	1.2	10.5
Cv2R.12102	Non-/partial	20	16	4	58	0	ND	ND	25	0	4	1	0	0	0	0	0	0	0	0	0	ND	ND	ND	ND	ND	ND	ND	ND	ND	ND	ND	ND	ND	ND	ND	ND	ND	ND	1.0	2.0	1.4	0.6
Cv2R.12115	Non-/partial	44	44	12	59	20	ND	ND	25	1	6	2	0	0	0	0	0	0	0	0	0	ND	ND	ND	ND	ND	ND	ND	ND	ND	ND	ND	ND	ND	ND	ND	ND	ND	ND	1.1	1.7	1.4	0.6
Cv2R.12116	Broad	100	100	61	54	97	27	19	94	6	56	87	94	80	10	5	89	93	0	0	37	0	0	1	3	0	1	10	51	23	0	1	4	49	2	1	1	5	1	1.3	16.7	2.0	8.2
Cv2R.12118	Non-/partial	78	54	27	46	46	28	11	2	1	1	0	63	15	43	28	45	40	1	0	40	ND	ND	ND	ND	ND	ND	ND	ND	ND	ND	ND	ND	ND	ND	ND	ND	ND	ND	1.3	2.3	1.6	1.0
Cv2R.12121	Non-/partial	14	10	0	29	0	ND	ND	25	1	0	5	0	0	0	0	0	0	0	0	0	ND	ND	ND	ND	ND	ND	ND	ND	ND	ND	ND	ND	ND	ND	ND	ND	ND	ND	1.1	1.1	1.6	1.0
Cv2R.12124	ND	ND	ND	ND	ND	ND	ND	ND	ND	ND	ND	ND	ND	ND	ND	ND	ND	ND	ND	ND	ND	ND	ND	ND	ND	ND	ND	ND	ND	ND	ND	ND	ND	ND	ND	ND	ND	ND	ND	ND	ND	ND	ND
Cv2R.12145	Broad	83	100	73	88	71	75	41	58	24	15	48	95	79	92	88	93	93	50	73	68	28	79	86	85	66	67	52	73	88	18	66	75	82	53	80	74	75	63	1.4	14.1	1.5	7.8
Cv2R.12153	ND	ND	ND	ND	ND	ND	ND	ND	ND	ND	ND	ND	ND	ND	ND	ND	ND	ND	ND	ND	ND	ND	ND	ND	ND	ND	ND	ND	ND	ND	ND	ND	ND	ND	ND	ND	ND	ND	ND	ND	ND	ND	ND
Cv2R.13104	Narrow	98	100	0	43	98	ND	ND	94	0	0	88	82	87	23	20	93	88	26	4	18	ND	ND	ND	ND	ND	ND	ND	ND	ND	ND	ND	ND	ND	ND	ND	ND	ND	ND	1.2	12.5	1.1	1.5
Cv2R.13114	Narrow	100	100	0	20	99	ND	ND	96	9	16	96	95	79	14	5	94	95	0	30	0	ND	ND	ND	ND	ND	ND	ND	ND	ND	ND	ND	ND	ND	ND	ND	ND	ND	ND	1.3	11.4	1.8	7.9
Cv2R.13129	Non-/partial	13	8	0	22	0	ND	ND	12	0	5	0	0	0	0	0	0	0	0	0	10	ND	ND	ND	ND	ND	ND	ND	ND	ND	ND	ND	ND	ND	ND	ND	ND	ND	ND	1.2	0.8	1.1	0.9
Cv2R.13133	Non-/partial	44	61	5	50	24	19	12	0	0	0	71	93	82	92	87	94	93	84	69	63	ND	ND	ND	ND	ND	ND	ND	ND	ND	ND	ND	ND	ND	ND	ND	ND	ND	ND	1.3	2.2	1.4	3.8
Cv2R.13145	Broad	66	58	57	70	61	17	8	16	1	0	0	91	26	76	61	84	86	0	61	8	0	3	84	22	63	5	1	2	82	26	6	14	13	42	74	69	63	66	1.2	3.0	1.5	3.3
Cv2R.13148	Non-/partial	46	34	32	63	49	ND	ND	15	3	2	0	0	6	10	0	38	21	0	0	26	ND	ND	ND	ND	ND	ND	ND	ND	ND	ND	ND	ND	ND	ND	ND	ND	ND	ND	1.2	1.5	1.1	11.4
Cv2R.13150	Non-/partial	8	0	0	34	0	ND	ND	12	1	0	0	0	0	0	0	0	0	0	0	0	ND	ND	ND	ND	ND	ND	ND	ND	ND	ND	ND	ND	ND	ND	ND	ND	ND	ND	1.4	0.9	1.1	1.0
Cv2R.13151	Broad	104	98	71	96	100	23	23	96	4	0	97	74	90	74	87	91	86	0	19	14	3	2	34	25	26	30	1	0	0	38	0	2	0	0	0	0	0	0	1.4	6.4	1.3	10.0
Cv2R.13152	Non-/partial	34	47	21	60	3	ND	ND	23	15	0	0	0	5	0	0	0	0	0	0	0	ND	ND	ND	ND	ND	ND	ND	ND	ND	ND	ND	ND	ND	ND	ND	ND	ND	ND	1.4	3.7	1.6	0.9
Cv2R.13159	Broad	83	85	89	80	87	92	93	84	78	48	32	52	35	33	0	37	4	18	0	34	78	2	0	0	1	0	1	0	0	1	0	2	0	0	0	0	0	0	1.5	7.1	2.6	0.8
Cv2R.13162	Broad	96	99	84	90	99	98	100	96	83	75	94	77	93	41	42	91	90	28	78	70	96	76	94	95	61	92	47	62	28	36	3	20	70	2	1	1	5	1	1.3	8.6	1.6	7.1
Cv2R.13164	Narrow	91	91	0	23	98	ND	ND	71	1	0	68	79	92	65	7	92	92	0	0	62	ND	ND	ND	ND	ND	ND	ND	ND	ND	ND	ND	ND	ND	ND	ND	ND	ND	ND	1.3	6.5	1.5	13.4
Cv2R.13168	Narrow	98	98	0	4	97	ND	ND	93	4	9	72	76	80	7	1	86	88	0	0	3	ND	ND	ND	ND	ND	ND	ND	ND	ND	ND	ND	ND	ND	ND	ND	ND	ND	ND	1.3	9.8	1.3	7.7
Cv2R.13181	Non-/partial	43	27	16	2	8	ND	ND	3	1	0	0	0	1	0	0	0	0	0	2	20	ND	ND	ND	ND	ND	ND	ND	ND	ND	ND	ND	ND	ND	ND	ND	ND	ND	ND	1.3	1.5	1.4	1.4
Cv2R.13184	Non-/partial	50	80	25	57	12	ND	ND	8	3	0	0	0	0	0	0	0	0	0	0	0	ND	ND	ND	ND	ND	ND	ND	ND	ND	ND	ND	ND	ND	ND	ND	ND	ND	ND	1.4	3.6	2.1	1.0
Cv2R.13203	ND	ND	ND	ND	ND	ND	ND	ND	ND	ND	ND	ND	ND	ND	ND	ND	ND	ND	ND	ND	ND	ND	ND	ND	ND	ND	ND	ND	ND	ND	ND	ND	ND	ND	ND	ND	ND	ND	ND	ND	ND	ND	ND
Cv2R.13204	Non-/partial	27	49	6	63	8	ND	ND	6	11	17	0	0	0	0	0	0	0	0	0	0	ND	ND	ND	ND	ND	ND	ND	ND	ND	ND	ND	ND	ND	ND	ND	ND	ND	ND	1.3	2.6	1.6	0.9
Cv2R.13207	Non-/partial	19	7	21	25	16	ND	ND	17	0	0	0	69	55	57	45	67	69	0	0	15	ND	ND	ND	ND	ND	ND	ND	ND	ND	ND	ND	ND	ND	ND	ND	ND	ND	ND	1.3	3.3	1.0	2.6
Cv2R.13214	Non-/partial	11	0	13	20	0	ND	ND	17	2	0	0	0	0	0	0	0	0	14	0	12	ND	ND	ND	ND	ND	ND	ND	ND	ND	ND	ND	ND	ND	ND	ND	ND	ND	ND	1.1	1.1	1.1	1.4
Cv2R.13216	Non-/partial	34	29	2	22	11	ND	ND	4	2	6	0	0	0	0	0	0	0	0	0	0	ND	ND	ND	ND	ND	ND	ND	ND	ND	ND	ND	ND	ND	ND	ND	ND	ND	ND	1.2	2.8	1.4	1.0
Cv2R.13217	Broad	81	79	72	99	67	16	5	36	5	4	11	82	88	86	84	90	91	16	0	4	0	0	0	0	1	0	0	0	4	1	0	0	1	0	0	0	0	0	1.2	3.0	1.2	11.6
Cv2R.13222	Narrow	100	98	11	37	95	ND	ND	64	2	1	67	77	91	0	0	90	88	0	0	14	ND	ND	ND	ND	ND	ND	ND	ND	ND	ND	ND	ND	ND	ND	ND	ND	ND	ND	1.4	5.1	1.2	8.9

ND, not determined; Wu., Wuhan; neut., neutralization; inh., inhibition; ACE2-mim., ACE2 memetic activity.